ISA Transactions 169 (2026) 302–317

Contents lists available at ScienceDirect

ISA Transactions

journal homepage: www.elsevier.com/locate/isatra

Research article

Looped functional approach to finite-horizon hybrid control for networked switched fuzzy systems with fault indicators and cyber attacks

N. Aravinth [a, b], R. Sakthivel [c,*], O.M. Kwon [a,*]

[a] School of Electrical Engineering, Chungbuk National University, Cheongju 28644, South Korea
[b] Department of Mathematics, Karpagam Academy of Higher Education, Coimbatore 641021, India
[c] Department of Applied Mathematics, Bharathiar University, Coimbatore 641046, India

HIGHLIGHTS

- Sampled hybrid control comprises the robust and fault-tolerant control which is designed.
- Finite horizon control via a two-sided looped functional technique is investigated.
- The fault-alarm mechanism is deployed to transition control whenever a fault appears.
- The hybrid cyber-attacks, which include deception and DoS attacks, are considered.

ARTICLE INFO

Keywords:
Networked Switched Fuzzy System
Hybrid Cyber Attacks
Two-sided Looped Functional
Fault Alarm
Hybrid Control
Finite-time Control

ABSTRACT

The presented research effort offers a secure sampled hybrid control design for networked switched fuzzy systems. Precisely, we investigate the challenges posed by actuator failures, hybrid cyber attacks, time-varying delays and external disturbances over the finite horizon. A unified control design that effectively handles these simultaneous factors in a single framework is an area that warrants investigation. In this connection, a hybrid control law which comprises the robust and fault-tolerant control is established. One of the primary appealing aspects of the designed control law is that it employs robust control when the system is free of faults and switches to the fault-tolerant one when the system encounters a fault. Further, by considering the state information from $\vartheta(t_{\mathfrak{k}})$ to $\vartheta(t)$ and $\vartheta(t)$ to $\vartheta(t_{\mathfrak{k}+1})$, a two-sided looped functional is developed. Based on that, adequate conditions that promise the core objective of this examination are formulated in terms of linear matrix inequality. Apart from this, to escalate the controller functionality in regard to cyber threats, hybrid cyber attacks that comprise the deception and denial-of-service attacks are taken into account and Bernoulli distribution is utilized to govern the random characteristics of the attack. Additionally, to address the repercussions of the external disturbance, extended dissipative theory is deployed. In the closing part, two examples, including the single-link robotic arm model accompanied by the simulation findings, are presented to showcase the capability and applicability of the achieved theoretical outcomes and control design.

1. Introduction

In recent times, switched systems have been deeply investigated on account of their scientific significance and prospective implications. Precisely, a variety of actual platforms with various modes can be simulated and scrutinized by switched systems, including airplane systems, traffic management systems, robotic systems and network-controlled systems [1]. Further, a switched system constitutes multiple subsystems and a switching mechanism that directs the transitions among them. Moreover, the subsystems have been coupled to capture the system's typical dynamics over its different operational modes, each activated by an appropriate switching signal. Additionally, the switching principle sets forth the interconnection of subsystems, specifying the exact subsystem designated to be activated at a given time. Furthermore, when a system experiences switching, relevant arbitrary switching rules can cause the entire system to become unstable, even though every single subsystem remains stable. The implication here is that the stability of

* Corresponding authors.
Email addresses: krsakthivel@buc.edu.in (R. Sakthivel), madwind@chungbuk.ac.kr (O.M. Kwon).

https://doi.org/10.1016/j.isatra.2025.12.014
Received 13 May 2025; Received in revised form 5 December 2025; Accepted 5 December 2025
Available online 12 December 2025

the subsystems and the overall system cannot be assured in a mutually exclusive manner. In this context, a notable approach for ensuring the stability of switched systems is the average dwell time method. Recent years have seen the introduction of a number of control planning and stability strategies for switched systems as well as the discovery of some intriguing insights [2,3] owing to its practical relevance. These factors establish the backdrop for the adoption of the switched system frameworks for the current investigation.

In turn, in the contemporary sector, nearly all engineering systems exhibit nonlinear dynamic properties attributable to intrinsic or environmental influences. In particular, multiple research efforts on nonlinear systems [4–6] have been comprehensively undertaken, as nonlinearity can lead to challenges in stability evaluation and control composition. Among these, the T-S fuzzy model delivers a productive approach for expressing intricate nonlinear systems employing fuzzy blending techniques. In detail, the T-S fuzzy paradigm enables nonlinear systems to be perceived as a convex amalgamation of many linear subsystems via membership functions. This strategy has culminated in the reporting of numerous firmly established outcomes for nonlinear systems, drawing from findings in linear systems. Owing to its crucial significance, the T-S fuzzy model has found widespread use in electrical structures, mass-spring systems and mechanical engineering. In recent years, a wealth of outstanding findings has appeared regarding T-S fuzzy systems [7,8]. Consequently, the study of switched nonlinear systems through the T-S fuzzy approach demonstrates greater applicability compared to the linear case. Resultantly, pertinent findings [9,10] on switched nonlinear plant frameworks utilizing the T-S fuzzy mechanism have been laid out across various areas. Given the rapid advances in control systems, the study of switched fuzzy systems merits further exploration, as combining switched dynamics with fuzzy modeling opens promising directions yet to be fully realized and thus motivates our choice of this system.

Whenever control industrial technology innovation advances, the control becomes increasingly intricate and the demand for control precision escalates to unprecedented levels. Simultaneously, actuator failures are inevitable on account of the delicate layout of present-day equipment and the demands of high-power, high-load continuous operation. In numerous instances, the malfunction of a single component may lead to a chain of significant repercussions. To combat this challenge, numerous academics have centered on fault-tolerant control [11,12]. Nevertheless, immediately putting the fault-tolerant controllers into operation will generate a somewhat conservative scheme, especially if the system doesn't possess any actuator shortcomings. Consequently, to resolve this issue, the academics have come up with hybrid control [13]. Specifically, the hybrid control technique has been developed by combining both robust and fault-tolerant controllers, which enhances the system functionality under both fault-free and fault-occurrence conditions. In detail, the robust controller is in operation when the system functions without actuator failures and the fault-tolerant controller will take over from the robust one if a problem arises. Further, the fault alarm methodology is employed to notify and stimulate the controller as soon as the system encounters a failure. Thus far, only a small number of hybrid control approaches [14] using fault alarm configurations have been explored. While fault alarm-based hybrid control has been formulated, its implementation in considered systems remains unestablished. The absence of a comprehensive framework prompts our investigation into this topic.

The tremendous advancement of digital monitoring technologies and the rapid development of intelligent devices in the past few years have led to the development of sampled data control techniques, which achieve higher levels of stability and reliability. Unquestionably, scientific inquiry on sampled-data control systems [15] has drawn a great deal of attention. In detail, sampled-data control involves recording system state insights at sampling instances and producing commands by holding onto the control signals from the current time till the next sampling moment via a zero-order hold. It eliminates the need for the system to continuously transmit state data, thus significantly lowering the amount of data transmitted and enhancing the usage of constrained frequencies. In recent times, a growing number of notable accomplishments have been documented in this area [16,17]. Even though the expense of installation and time can be reduced using a sampled-data control approach, the closed-loop system's dynamical modelling becomes more complex. Specifically, the study and development of sampled-data control systems has been approached from multiple directions: discretization [18], impulsive systems formulation [19], the input delay approach [20] and looped functional [21]. The looped functional approach stands out among the rest as a modern method. It differs from other approaches in the way that it solely requires the functional to be positive at the sampling moments, rather than during the complete sample interval. It has the potential to increase the maximum sample intervals while decreasing the conservatism. By employing the looped-functional technique, next-generation studies on different systems have been examined [22,23]. Continuous development of this idea has led to the creation of a two-sided looped functional [24–26] that takes state data into account within the intervals $\vartheta(t_k)$ and $\vartheta(t)$ and $\vartheta(t)$ to $\vartheta(t_{k+1})$. Acquainted by its distinctive features, a framework of sampled-data control using the two-sided looped functional is essential and this gap motivates the present study and defines its focus.

The relentless enhancement of contemporary technology has culminated in increasingly sophisticated cyber attacks, hence posing a growing threat to the system. Presently, more than 20 forms of cyber attacks have been identified; nevertheless, the predominant focus of research has been on deception attacks [28] and denial-of-service (DoS) attacks [29]. Specifically, DoS attacks have the goal of obstructing legitimate clients from acquiring the system or impairing its operational capacity. Whereas, deception attacks pertain to the clandestine introduction of incorrect or deceptive data into the system, typically via compromised sensors or communication channels. Furthermore, it is essential to note that attackers prefer to amplify the adverse impacts of their operations by utilizing a combination of multiple avenues in coordinated cyber attacks. Consequently, the security issues related to hybrid cyber attacks are now receiving significant scholarly attention from academics in the field of control society [30,31]. Nevertheless, investigations into hybrid cyber attacks on the system being targeted remain in the early stages of development, requiring additional examination and serving as an impulse for this study.

Meanwhile, the idea of Lyapunov stability is frequently examined within the domain of system stability theory. Specifically, it involves analyzing the dynamic properties of a system over an unlimited time frame, so encapsulating the system's steady-state behavior over an infinite time horizon. In many real-world situations, it is occasionally essential for control systems to deliver a consistent response in the quickest possible time. In this scenario, control strategies that operates indefinitely are incapable of fulfilling system requirements owing to their propensity for creating extended transient outputs. Thereby, the finite-time stability theory is put forth [32] as an avenue to adequately address the previously discussed concerns. Notably, the implemented system functionality is confined to a specified finite-time frame instead of an indefinite duration. Recently, the curiosity regarding exploring the subject of finite-time stability has increased [33,34], solely owing to its practical significance. The aforementioned intriguing features have drawn us to investigate the finite-time stability for the system in question.

Despite significant advances in the study of the undertaken system, the following challenges remain unresolved. First, actuator faults and cyber attacks often occur concurrently in networked settings, whereas most treatments handle them separately, yielding brittle resilience. Second, although the two-sided looped functional has the potential to exploit both pre-and post-sample information, its application to sampled hybrid control of investigated systems is still underexplored, leaving design conditions incomplete. Third, incorporating hybrid cyber attacks that combine deception and DoS attacks patterns introduces randomness and unpredictability, making analysis and control design more complex.

These interrelated challenges outline the primary obstacle that propels our inquiry.

Bringing impetus to the preceding discoveries and research necessities, the current study deals with the sampled hybrid control design problem for networked switched fuzzy systems (NSFSs) in the backdrop of various susceptible elements. The excerpts that follow are brief summary of the significant findings of this investigation:

- The sampled hybrid control design issue for the NSFSs in the context of actuator faults, hybrid cyber attacks, time-varying delays and external disturbances over a finite horizon through the two-sided looped functional technique is investigated.
- In detail, a sampled hybrid control design that comprises the robust and fault-tolerant control is formulated. The fault alarm mechanism is deployed to facilitate the controller to transition between robust and fault-tolerant modes whenever a fault appears.
- The requisite constraints that are insuring the primary goal of this investigation are established with the assist of finite-time stability theory and linear matrix inequality (LMI). Precisely, a two-sided looped-based Lyapunov functional is developed wherein the sample intervals $\vartheta(t_k)$ to $\vartheta(t)$ and $\vartheta(t)$ to $\vartheta(t_{k+1})$ are considered which escalates the functioning of the controller.
- The hybrid cyber attacks, which includes deception and DoS attacks, are factored into account with the goal to boost the safety of the data in networks. Further, to address the footprints of disturbances, extended dissipative theory is deployed.
- In closing, the research wraps up with two numerical examples, including a single-link robot arm model, along with the computational findings to show off the capability and practicality of the created control law and documented theoretical findings.

Paper Organization: The rest of the paper is organized as follows. Section 2 presents the problem formulation and preliminaries. Section 3 provides the main results, including finite-time analysis and hybrid control design. Section 4 illustrates the effectiveness of the proposed method through numerical simulations. Section 5 concludes the paper with key findings and future directions.

Notations: $\mathbb{R}^{\vartheta}$ denotes the ϑ-dimensional Euclidean space. The expression $\mathcal{P} > 0$ implies that the matrix $\mathcal{P}$ is positive definite. $\mathcal{P}^T$ epitomizes the transpose of the matrix $\mathcal{P}$. $Sym\{\mathcal{P}\}$ represents the sum of $\mathcal{P}$ and its transpose matrix $\mathcal{P}^T$. I means the Identity matrix. $\Upsilon^{r,h}$(or $\Upsilon_{r,h}$) represents the corresponding $r-th$ row and $h-th$ column elements of the matrix Υ. The symbol asterisk (*) indicate that the elements caused by symmetry. $diag\{.\}$ signifies for the block diagonal matrix.

2. Problem formulation

This portion offers the mathematical modelling of the undertaken system subject to multiple vulnerable factors, control design and preliminaries. In this connection, first let us consider the nonlinear switched system in the following manner:

$$\begin{aligned}\dot{\vartheta}(t) &= f_{\zeta(t)}(\vartheta(t), \lambda(t), \delta(t)),\\ \xi(t) &= \mathfrak{g}_{\zeta(t)}(\vartheta(t)).\end{aligned} \tag{1}$$

By deploying the T-S fuzzy notion, the above given nonlinear switched system along with the time-varying delay can be transformed into the ensuing form:

Plant Rule $\mathfrak{d}$: **IF** $\mathfrak{E}_1(t)$ is $\mathfrak{M}_{\zeta(t)1\mathfrak{d}}$, $\mathfrak{E}_2(t)$ is $\mathfrak{M}_{\zeta(t)2\mathfrak{d}}$, …, $\mathfrak{E}_r(t)$ is $\mathfrak{M}_{\zeta(t)r\mathfrak{d}}$, **THEN**

$$\begin{aligned}\dot{\vartheta}(t) &= \mathfrak{A}_{\zeta(t)\mathfrak{d}}\vartheta(t) + \mathfrak{V}_{\zeta(t)\mathfrak{d}}\vartheta(t-\imath(t)) + \mathfrak{B}_{\zeta(t)\mathfrak{d}}\lambda(t) + \mathfrak{D}_{\zeta(t)\mathfrak{d}}\delta(t),\\ \xi(t) &= \mathfrak{C}_{\zeta(t)\mathfrak{d}}\vartheta(t),\\ \vartheta(t_0) &= \tilde{\vartheta}(t_0),\ \forall t_0 \in [-\bar{\imath}, 0],\end{aligned} \tag{2}$$

where $\mathfrak{E}_1(t), \mathfrak{E}_2(t), \dots, \mathfrak{E}_r(t)$ and $\mathfrak{M}_{\zeta(t)1\mathfrak{d}}, \mathfrak{M}_{\zeta(t)2\mathfrak{d}}, \dots, \mathfrak{M}_{\zeta(t)r\mathfrak{d}}$, $\mathfrak{d} = \{1, 2, \dots, \mathfrak{q}\}$ are the premise variables and fuzzy sets, respectively; $\mathfrak{q}$ stands for the number of IF-THEN rules; r represents the number of premise variables; $\zeta(t) : \mathbb{R}^+ \to \mathcal{M} = \{1, 2, \dots, \mathfrak{m}\}$ epitomizes the switching law that takes values in a finite set and $\mathfrak{m} > 1$; $\vartheta(t) \in \mathbb{R}^x$, $\lambda(t) \in \mathbb{R}^u$ and $\xi(t) \in \mathbb{R}^z$ indicate the state, control and output vector of the undertaken model; $\delta(t) \in \mathcal{L}_2[0, \infty)$ depicts the external disturbances; $\imath(t)$ denotes the time-varying delay in the investigated model with the following constraint $\bar{\imath} > \imath(t) > 0$ and $i(t) \le \kappa < 1$; For the notation brevity, the switching signal $\zeta(t)$ is indicated as $\mathfrak{j}$. Subsequently, by using the fuzzy blending method, the system (2) can reformulated as in the below manner:

$$\begin{aligned}\dot{\vartheta}(t) &= \sum_{\mathfrak{d}=1}^{\mathfrak{q}} \mathfrak{h}_{\mathfrak{j}\mathfrak{d}}(\mathfrak{E}(t))\big[\mathfrak{A}_{\mathfrak{j}\mathfrak{d}}\vartheta(t) + \mathfrak{V}_{\mathfrak{j}\mathfrak{d}}\vartheta(t-\imath(t)) + \mathfrak{B}_{\mathfrak{j}\mathfrak{d}}\lambda(t) + \mathfrak{D}_{\mathfrak{j}\mathfrak{d}}\delta(t)\big],\\ \xi(t) &= \sum_{\mathfrak{d}=1}^{\mathfrak{q}} \mathfrak{h}_{\mathfrak{j}\mathfrak{d}}(\mathfrak{E}(t))\big[\mathfrak{C}_{\mathfrak{j}\mathfrak{d}}\vartheta(t)\big],\end{aligned} \tag{3}$$

where $\mathfrak{h}_{\mathfrak{j}\mathfrak{d}}(\mathfrak{E}(t)) = \mathfrak{l}_{\mathfrak{j}r} / \sum_{\mathfrak{d}=1}^{\mathfrak{q}} \mathfrak{l}_{\mathfrak{j}\mathfrak{d}}$, $\mathfrak{l}_{\mathfrak{j}r} = \prod_{\mathfrak{p}=1}^{\mathfrak{q}} \mathfrak{M}_{\mathfrak{j}\mathfrak{p}\mathfrak{d}}(\mathfrak{E}_{j\mathfrak{p}}(t))$ in this $\mathfrak{M}_{\mathfrak{j}\mathfrak{p}\mathfrak{d}}(\mathfrak{E}_{\mathfrak{j}\mathfrak{p}}(t))$ constitutes the membership grade of $\mathfrak{E}_{\mathfrak{j}\mathfrak{p}}(t)$ in $\mathfrak{M}_{\mathfrak{j}\mathfrak{p}\mathfrak{d}}$ and $\mathfrak{h}_{\mathfrak{j}\mathfrak{d}}(\mathfrak{E}(t)) \ge 0$, $\sum_{\mathfrak{d}=1}^{\mathfrak{q}} \mathfrak{h}_{\mathfrak{j}\mathfrak{d}}(\mathfrak{E}(t)) = 1$.

Subsequently, to ease the derivation, the following notations are introduced for the system matrices as in the ensuing form: $\tilde{\mathfrak{A}}_{\mathfrak{j}\mathfrak{d}} = \sum_{\mathfrak{d}=1}^{\mathfrak{q}} \mathfrak{h}_{\mathfrak{j}\mathfrak{d}}(\mathfrak{E}(t))\mathfrak{A}_{\mathfrak{j}\mathfrak{d}}$, $\tilde{\mathfrak{V}}_{\mathfrak{j}\mathfrak{d}} = \sum_{\mathfrak{d}=1}^{\mathfrak{q}} \mathfrak{h}_{\mathfrak{j}\mathfrak{d}}(\mathfrak{E}(t))\mathfrak{V}_{\mathfrak{j}\mathfrak{d}}$, $\tilde{\mathfrak{B}}_{\mathfrak{j}\mathfrak{d}} = \sum_{\mathfrak{d}=1}^{\mathfrak{q}} \mathfrak{h}_{\mathfrak{j}\mathfrak{d}}(\mathfrak{E}(t))\mathfrak{B}_{\mathfrak{j}\mathfrak{d}}$, $\tilde{\mathfrak{D}}_{\mathfrak{j}\mathfrak{d}} = \sum_{\mathfrak{d}=1}^{\mathfrak{q}} \mathfrak{h}_{\mathfrak{j}\mathfrak{d}}(\mathfrak{E}(t))\mathfrak{D}_{\mathfrak{j}\mathfrak{d}}$, $\tilde{\mathfrak{C}}_{\mathfrak{j}\mathfrak{d}} = \sum_{\mathfrak{d}=1}^{\mathfrak{q}} \mathfrak{h}_{\mathfrak{j}\mathfrak{d}}(\mathfrak{E}(t))\mathfrak{C}_{\mathfrak{j}\mathfrak{d}}$. Then, by using these indications, the system (3) can be framed as in the beneath compact form:

$$\begin{aligned}\dot{\vartheta}(t) &= \tilde{\mathfrak{A}}_{\mathfrak{j}\mathfrak{d}}\vartheta(t) + \tilde{\mathfrak{V}}_{\mathfrak{j}\mathfrak{d}}\vartheta(t-\imath(t)) + \tilde{\mathfrak{B}}_{\mathfrak{j}\mathfrak{d}}\lambda(t) + \tilde{\mathfrak{D}}_{\mathfrak{j}\mathfrak{d}}\delta(t),\\ \xi(t) &= \tilde{\mathfrak{C}}_{\mathfrak{j}\mathfrak{d}}\vartheta(t).\end{aligned} \tag{4}$$

2.1. Configuration of sampled control with hybrid cyber attacks

Let $\{t_0, t_1, t_2, \dots, t_{\mathfrak{k}}, \dots\}$ be a sequence of sampling instances and the states of the undertaken model can be obtained only in the sampling instant $t_{\mathfrak{k}}$. Then, the sampled-data controller is formulated based on the parallel distributed compensation strategy as follows:

Control rule ν: **IF** $\mathfrak{E}_1(t)$ is $\mathfrak{M}_{\zeta(t)1\nu}$, $\mathfrak{E}_2(t)$ is $\mathfrak{M}_{\zeta(t)2\nu}$, …, $\mathfrak{E}_r(t)$ is $\mathfrak{M}_{\zeta(t)r\nu}$, **THEN**

$$\lambda(t) = \sum_{\nu=1}^{\mathfrak{q}} \mathfrak{h}_{\mathfrak{j}\nu}(\mathfrak{E}(t))\mathfrak{H}_{\mathfrak{j}\nu}\vartheta(t_{\mathfrak{k}}), t \in [t_{\mathfrak{k}}, t_{\mathfrak{k}+1}), \tag{5}$$

where $\mathfrak{H}_{\mathfrak{j}\nu}$ is the controller gain matrix that will be discussed in the later segment; $t_{\mathfrak{k}}$ signifies the sampling instant and $0 < \mathfrak{y}_1 \le t_{\mathfrak{k}+1} - t_{\mathfrak{k}} = \mathfrak{y}_{\mathfrak{k}} \le \mathfrak{y}_2$ wherein $\mathfrak{y}_1$ and $\mathfrak{y}_2$ represent the lower and upper bounds of the sampling interval respectively.

Subsequently, given the significance of the arbitrary attacks inside the network circumstances, a hybrid attack strategy is formed, encompassing both deception and DoS attacks, whereby the deception attack utilize bogus data in lieu of authentic data to undermine the operation of the control model. At first, when the implemented system experiences only a deception attack, model (5) can be formulated as follows:

$$\lambda(t) = \sum_{\nu=1}^{\mathfrak{q}} \mathfrak{h}_{\mathfrak{j}\nu}(\mathfrak{E}(t))\mathfrak{H}_{\mathfrak{j}\nu}\big[\alpha(t)\mathfrak{f}(\vartheta(t_{\mathfrak{k}})) + (1-\alpha(t))\vartheta(t_{\mathfrak{k}})\big]. \tag{6}$$

Simultaneously, a DoS attack indicates that the transfer of signals is significantly obstructed. Then, control (6) can be modified as

$$\lambda(t) = \sum_{\nu=1}^{\mathfrak{q}} \mathfrak{h}_{\mathfrak{j}\nu}(\mathfrak{E}(t))\mathfrak{H}_{\mathfrak{j}\nu}\beta(t)\big[\alpha(t)\mathfrak{f}(\vartheta(t_{\mathfrak{k}})) + (1-\alpha(t))\vartheta(t_{\mathfrak{k}})\big], \tag{7}$$

wherein $\alpha(t)$ and $\beta(t)$ signify the state of the occurrence of deception and DoS attacks, respectively and they are assumed to be independent

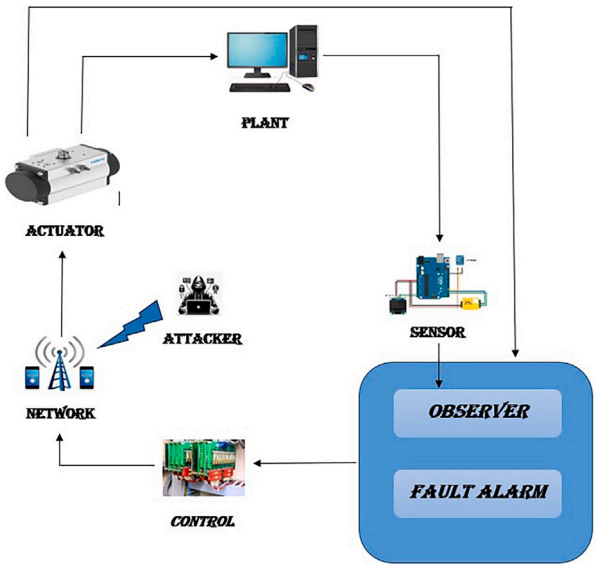

Fig. 1. Schematic representation of presented control law and the component illustrations used here are adapted from [26,27] and publicly available resources.

from one another. Precisely, when $\beta(t) = 0$ irrespective of whether the deception attack takes place or not, the network framework is blocked, then the control $\lambda(t) = 0$. In turn, when $\alpha(t) = 1$ and $\beta(t) = 1$, the actual signal $\vartheta(t_{\mathfrak{k}})$ is replaced by the nonlinear malicious signal $\mathfrak{f}(\vartheta(t_{\mathfrak{k}}))$ which implies $\lambda(t) = \sum_{\nu=1}^{\mathfrak{q}} \mathfrak{h}_{\mathfrak{j}\nu}(\mathfrak{E}(t))\mathfrak{H}_{\mathfrak{j}\mathfrak{d}}\mathfrak{f}(\vartheta(t_{\mathfrak{k}}))$. Moreover, when $\alpha(t) = 0$ and $\beta(t) = 1$, then there is no attack taking place in the control channel.

Remark 1. In the actual realm of technology, the network environment is vulnerable to malicious network attacks, which is one of the primary characteristics harming the safety of networks. In this investigation, it is assumed that communication networks are under attack from a variety of cyber threats. To be more specific, cyber attacks exhibit the arbitrary traits. As a result, Bernoulli sequences with predetermined statistical significance are deemed to ensure both the deception and DoS attacks and the statistical properties are as follows: $\mathbb{E}\{\alpha(t)\} = Pr\{\alpha(t) = 1\} = \bar{\alpha}$ and $\mathbb{E}\{\beta(t)\} = Pr\{\beta(t) = 1\} = \bar{\beta}$.

Thereafter, by employing the designed control law (7) and denoting $\tilde{\mathfrak{H}}_{\mathfrak{j}\nu} = \sum_{\nu=1}^{\mathfrak{q}} \mathfrak{h}_{\mathfrak{j}\nu}(\mathfrak{E}(t))\mathfrak{H}_{\mathfrak{j}\nu}$, the closed-loop framework is obtained as follows:

$$\begin{aligned}\dot{\vartheta}(t) =& \tilde{\mathfrak{A}}_{\mathfrak{j}\mathfrak{d}}\vartheta(t) + \tilde{\mathfrak{V}}_{\mathfrak{j}\mathfrak{d}}\vartheta(t-\imath(t)) + \tilde{\mathfrak{B}}_{\mathfrak{j}\mathfrak{d}}\beta(t)\{\tilde{\mathfrak{H}}_{\mathfrak{j}\nu}\alpha(t)\mathfrak{f}(\vartheta(t_{\mathfrak{k}})) \\ &+ (1-\alpha(t))\tilde{\mathfrak{H}}_{\mathfrak{j}\nu}\vartheta(t_{\mathfrak{k}})\} + \tilde{\mathfrak{D}}_{\mathfrak{j}\mathfrak{d}}\delta(t), \qquad (8)\\ \xi(t) =& \tilde{\mathfrak{C}}_{\mathfrak{j}\mathfrak{d}}\vartheta(t).\end{aligned}$$

Furthermore, the schematic representation of the presented control law is offered in Fig. 1

2.2. Preliminaries

Prior to entering the key findings section, it is imperative to lay out the subsequent assumptions, lemmas and definitions to facilitate the construction of appropriate constraints.

Assumption 1. The external disturbance $\delta(t)$ is presumed to be time-varying and it aligns with the criteria $\int_0^{\mathcal{G}_{\mathfrak{w}}} \delta^T(s)\delta(s)ds \le \delta_b$, where δ_b is a positive scalar.

Assumption 2. The deception attack function $\mathfrak{f}(\vartheta(t))$ is supposed to obey the following constraint:

$$||\mathfrak{f}(\vartheta(t))||_2 \le ||\mathcal{F}\vartheta(t)||_2,$$

where $\mathcal{F}$ indicates the upper bound of the function $\mathfrak{f}(\vartheta(t))$.

Assumption 3. For the stated time constant $\mathcal{G}_{\mathfrak{w}}$, the state vector of considered system $\vartheta(t)$ is time-varying and it meets the following constraint:

$$\int_0^{\mathcal{G}_{\mathfrak{w}}} \vartheta^T(s)\vartheta(s)ds \le \mathsf{k},$$

where k indicates the sufficient large constant value which is fixed.

Assumption 4. For the matrices $\mathcal{F}_1$, $\mathcal{F}_2$, $\mathcal{F}_3$ and $\mathcal{F}_4$, the ensuing requirements are obeyed:

- $\mathcal{F}_1 = \mathcal{F}_1^T \le 0$, $\mathcal{F}_3 = \mathcal{F}_3^T > 0$, $\mathcal{F}_4 = \mathcal{F}_4^T \ge 0$;
- $(\| \mathcal{F}_1 \| + \| \mathcal{F}_2 \|)\mathcal{F}_4 = 0$.

Assumption 5. For scalars $\gamma \ge 0, \mathfrak{i} \ge 1$ and t which belongs to the interval $[0, \mathcal{G}_{\mathfrak{w}}]$, we have

$$e^{\gamma t}\mathfrak{i}^{\mathcal{N}_{\mathfrak{j}}(0,t)} \le \mathsf{a},$$

where $\mathfrak{i}^{\mathcal{N}_{\mathfrak{j}}(0,t)}$ represents the switching number of $\zeta(t)$ over $(0,t)$ and a denotes a positive number.

Definition 1. [35] For the defined positive scalars $\mathcal{C}_1, \mathcal{C}_2$ and $\mathcal{G}_{\mathfrak{w}}$ with $\mathcal{C}_1 < \mathcal{C}_2$, the investigated system (4) is stated to be finite-time bounded in regard to $(\mathcal{C}_1, \mathcal{C}_2, \mathcal{G}_{\mathfrak{w}}, \delta_b, \mathcal{D})$, if

$$\sup_{-\bar{\imath}\le t_0<0} \mathbb{E}\{\vartheta^T(t_0)\mathcal{D}\vartheta(t_0)\} \le \mathcal{C}_1 \implies \mathbb{E}\{\vartheta^T(t)\mathcal{D}\vartheta(t)\} < \mathcal{C}_2,$$

where $\mathcal{D}$ is the positive definite matrix.

Definition 2. [35] For the state matrices $\mathcal{F}_1$, $\mathcal{F}_2$, $\mathcal{F}_3$ and $\mathcal{F}_4$ under the Assumption 4, the system (4) is said to be extended dissipative under zero initial constraint, the following connection holds:

$$\mathbb{E}\left\{ \int_0^{\mathcal{G}_{\mathfrak{w}}} \mathcal{H}(t)dt - \sup_{0\le t\le \mathcal{G}_{\mathfrak{w}}} \xi^T(t)\mathcal{F}_4\xi(t) \right\} \ge 0,$$

where $\mathcal{H}(t) = \xi^T(t)\mathcal{F}_1\xi(t) + 2\xi^T(t)\mathcal{F}_2\delta(t) + \delta^T(t)\mathcal{F}_3\delta(t)$.

Remark 2. It's worth to underscoring that the Assumption 4 leads to various performance indices, as demonstrated by the ensuing table, when $\mathcal{F}_1$, $\mathcal{F}_2$, $\mathcal{F}_3$ and $\mathcal{F}_4$ are each stated to various values:

Criteria	Performance index
$\mathcal{F}_1 = 0$, $\mathcal{F}_2 = 0$, $\mathcal{F}_3 = \eta^2\mathtt{I}$ and $\mathcal{F}_4 = \mathtt{I}$	$\mathtt{l}_2$-$\mathtt{l}_\infty$ Performance
$\mathcal{F}_1 = -\mathtt{I}$, $\mathcal{F}_2 = 0$, $\mathcal{F}_3 = \eta^2\mathtt{I}$ and $\mathcal{F}_4 = 0$	$\mathtt{H}_\infty$ Performance
$\mathcal{F}_1 = 0$, $\mathcal{F}_2 = \mathtt{I}$, $\mathcal{F}_3 = \eta\mathtt{I}$ and $\mathcal{F}_4 = 0$	Passivity Performance
$\mathcal{F}_1 = \mathcal{Q}$, $\mathcal{F}_2 = \mathcal{S}$, $\mathcal{F}_3 = \mathcal{R} - \zeta\mathtt{I}$ and $\mathcal{F}_4 = 0$	$(\mathcal{Q}, \mathcal{S}, \mathcal{R})$-Dissipativity Performance

Lemma 1. *[23] For any matrices $\mathcal{T} > 0$, $\mathcal{W}_1$, $\mathcal{W}_2$ and vector $\theta(t) \in \mathbb{R}^\theta$ and a differentiable function $\vartheta : [o_1, o_2] \to \mathbb{R}^r$, the underneath connection holds:*

$$\begin{aligned}-\int_{o_1}^{o_2} \dot{\vartheta}^T(s)\mathcal{T}\dot{\vartheta}(s)ds \le& (o_2-o_1)\theta^T(t)\Big[\mathcal{W}_1^T\mathcal{T}^{-1}\mathcal{W}_1 + \frac{(o_2-o_1)^2}{3}\mathcal{W}_2^T\mathcal{T}^{-1}\mathcal{W}_2\Big]\theta(t) \\ &+ 2\theta^T(t)\Big[\mathcal{W}_1^T(\vartheta(o_2)-\vartheta(o_1)) - 2\mathcal{W}_2^T\int_{o_1}^{o_2}\vartheta(r)dr\Big] \\ &+ 2(o_2-o_1)\theta^T(t)\mathcal{W}_2^T\big[\vartheta(o_2)+\vartheta(o_1)\big].\end{aligned}$$

Lemma 2. *[36] For any positive definite matrices $\mathcal{P}$, pre-defined positive scalars $\mathfrak{v}_1$, $\mathfrak{v}_2$ obeying $\mathfrak{v}_1 < \mathfrak{v}_2$ and the continuously differentiable function ϑ: $[\mathfrak{v}_1, \mathfrak{v}_2] \to \mathbb{R}^\vartheta$, the ensuing constraint is fulfilled:*

$$\int_{\mathfrak{v}_1}^{\mathfrak{v}_2} \vartheta^T(s)\mathcal{P}\vartheta(s)ds \ge \frac{1}{(\mathfrak{v}_2-\mathfrak{v}_1)}\mathfrak{I}^T(t)\mathcal{N}\mathfrak{I}(t),$$

where $\mathcal{N} = \begin{bmatrix} 9\mathcal{P} & -\frac{36}{\mathfrak{v}_2-\mathfrak{v}_1}\mathcal{P} & \frac{60}{(\mathfrak{v}_2-\mathfrak{v}_1)^2}\mathcal{P} \\ * & \frac{192}{(\mathfrak{v}_2-\mathfrak{v}_1)^2}\mathcal{P} & -\frac{360}{(\mathfrak{v}_2-\mathfrak{v}_1)^3}\mathcal{P} \\ * & * & \frac{720}{(\mathfrak{v}_2-\mathfrak{v}_1)^4}\mathcal{P} \end{bmatrix}$, $\mathfrak{I}^T(t) = \begin{bmatrix} \mathfrak{I}_1(t) & \mathfrak{I}_2(t) & \mathfrak{I}_3(t) \end{bmatrix}$, $\mathfrak{I}_1(t) = \int_{\mathfrak{v}_1}^{\mathfrak{v}_2} \vartheta^T(\mathfrak{s})d\mathfrak{s}$, $\mathfrak{I}_2(t) = \int_{\mathfrak{v}_1}^{\mathfrak{v}_2} d\mathfrak{s}\int_{\mathfrak{a}}^{\mathfrak{s}} \vartheta^T(\mathfrak{u})d\mathfrak{u}$, $\mathfrak{I}_3(t) = \int_{\mathfrak{v}_1}^{\mathfrak{v}_2} d\mathfrak{s}\int_{\mathfrak{a}}^{\mathfrak{s}} d\mathfrak{u}\int_{\mathfrak{a}}^{\mathfrak{u}} \vartheta^T(\mathfrak{v})d\mathfrak{v}$.

Remark 3. In [10], finite-time regulation of switched fuzzy systems is examined via mode-dependent Lyapunov functions under external disturbances. And, in [12], an output-feedback fault-tolerant scheme for nonlinear switched systems with full-state constraints is developed; it prioritizes constraint satisfaction and fault resilience. By contrast, the current study concentrates on handling network security and sampling-interval design. Specifically, we constructed a two-sided looped Lyapunov functional that explicitly treats the intervals $\vartheta(t_\mathfrak{k})$ to $\vartheta(t)$ and $\vartheta(t)$ to $\vartheta(t_{\mathfrak{k}+1})$, enabling longer admissible sampling gaps and improved efficiency. We devised a hybrid controller that blends robust and fault-tolerant modes, with a fault alarm trigger to switch seamlessly when faults arise. The control channel is modeled under hybrid cyber attack scenarios, adding security considerations. Altogether, the framework jointly advances performance, sampling-instance, fault tolerance and cyber resilience within a single design.

3. Main results

The present section unveils the requisite conditions that ensure the extended dissipative and finite-time boundedness of the system under examination. Precisely, we develop a two-sided looped Lyapunov functional and we deploy the LMI approach. Specifically, the first theorem sets out the appropriate requirements for the known gain matrices under a fault-free environment. Thereafter, accomplished results are further expanded to the unknown gain matrices and actuator failure circumstance. At the end, we present the constraints for detecting the fault and hybrid control law configuration.

For conciseness, the subsequent nomenclature is employed to streamline vector and matrix expressions: $\Phi_l = \begin{bmatrix} 0_{x\times(l-1)x} & I_x & 0_{x\times(13-l)x} \end{bmatrix}$, $(l = 1,2,\dots,13)$, $\Upsilon_1(t) = \int_{t_\mathfrak{k}}^{t} \vartheta(s)ds$, $\Upsilon_2(t) = \int_{t}^{t_\mathfrak{k}+1} \vartheta(s)ds$, $\Upsilon_3(t) = \vartheta(t) - \vartheta(t_\mathfrak{k})$, $\Upsilon_4(t) = \vartheta(t) - \vartheta(t_{\mathfrak{k}+1})$, $\aleph_1(t) = col\left\{\Upsilon_3(t), \Upsilon_1(t)\right\}$, $\aleph_2(t) = col\left\{\Upsilon_4(t), \Upsilon_2(t)\right\}$, $\aleph_3(t) = col\left\{\vartheta(t_\mathfrak{k}), \vartheta(t_{\mathfrak{k}+1})\right\}$, $\mathcal{W}_a = \left[\mathcal{W}_{a1}, \mathcal{W}_{a2}, \dots, \mathcal{W}_{a9}, 0, \mathcal{W}_{a11}, \mathcal{W}_{a12}, \mathcal{W}_{a13}\right]$, $\mathcal{W}_b = \left[\mathcal{W}_{b1}, \mathcal{W}_{b2}, \dots, \mathcal{W}_{b9}, 0\mathcal{W}_{b11}, \mathcal{W}_{b12}, \mathcal{W}_{b13}\right]$, $\mathcal{V}_a = \left[\mathcal{V}_{a1}, \mathcal{V}_{a2}, \dots, \mathcal{V}_{a9}, 0, \mathcal{V}_{a11}, \mathcal{V}_{a12}, \mathcal{V}_{a13}\right]$, $\mathcal{V}_b = \left[\mathcal{V}_{b1}, \mathcal{V}_{b2}, \dots, \mathcal{V}_{b9}, 0, \mathcal{V}_{b11}, \mathcal{V}_{b12}, \mathcal{V}_{b13}\right]$ and $\theta^T(t) = col\Big\{ \vartheta(t),\ \vartheta(t-\bar{\imath}(t)),\ \vartheta(t-\bar{\imath}),\ \vartheta(t_\mathfrak{k}),\ \vartheta(t_{\mathfrak{k}+1}),\ \Upsilon_1(t), \Upsilon_2(t),\ \dot{\vartheta}(t),\ \mathfrak{f}(\vartheta(t_\mathfrak{k})),\ \delta(t),\ \int_{t-\bar{\imath}}^{t}\vartheta(s)ds, \int_{t-\bar{\imath}}^{t}\int_{t-\bar{\imath}}^{s}\vartheta(v)dvds, \int_{-\bar{\imath}}^{0}\int_{t-\bar{\imath}}^{t+s}\int_{t-\bar{\imath}}^{t+v}\vartheta(w)dw\, dvds \Big\}$.

3.1. Finite-time bounded analysis for the NSFSs

Theorem 1. *Let the scalars $\bar{\imath}, \kappa, \mathfrak{y}_1, \mathfrak{y}_2, \bar{\alpha}, \bar{\beta}, \wp$ be predefined and Assumption 2 holds. For known gain matrices of controller $\tilde{\mathfrak{H}}_{\mathfrak{j}\nu}$, if there exist matrices $\mathcal{P}_{\mathfrak{e}\mathfrak{j}} > 0$, $\mathcal{Q}_{\mathfrak{e}\mathfrak{j}}$ $(\mathfrak{e} = 1,2,3,4)$, $\mathcal{S}_\mathfrak{j}$, $\mathcal{T}_{1\mathfrak{j}} > 0$ and $\mathcal{T}_{2\mathfrak{j}} > 0$, then the closed-loop framework (8) is stated to be finite-time bounded with respect to $(C_1, C_2, \mathcal{G}_\mathfrak{w}, \gamma, \mathcal{D})$, such that the below-given constraints hold:*

$$\begin{bmatrix} \Xi_1^{\mathfrak{d}\nu} + \mathfrak{y}_\mathfrak{k}\Xi_2^{\mathfrak{d}\nu} & \sqrt{\mathfrak{y}_\mathfrak{k}}\mathcal{V}_a^T & \sqrt{\mathfrak{y}_\mathfrak{k}\mathfrak{y}_2}\mathcal{V}_b^T \\ * & -\mathcal{T}_{2j} & 0 \\ * & * & -3\mathcal{T}_{2j} \end{bmatrix} < 0, \tag{9}$$

$$\begin{bmatrix} \Xi_1^{\mathfrak{d}\nu} + \mathfrak{y}_\mathfrak{k}\Xi_3^{\mathfrak{d}\nu} & \sqrt{\mathfrak{y}_\mathfrak{k}}\mathcal{W}_a^T & \sqrt{\mathfrak{y}_\mathfrak{k}\mathfrak{y}_2}\mathcal{W}_b^T \\ * & -\mathcal{T}_{1j} & 0 \\ * & * & -3\mathcal{T}_{1j} \end{bmatrix} < 0, \tag{10}$$

$$\mathcal{P}_{\mathfrak{e}\mathfrak{j}} < \mathfrak{i}\mathcal{P}_{\mathfrak{e}\varsigma},\ \mathcal{Q}_{\mathfrak{e}\mathfrak{j}} < \mathfrak{i}\mathcal{Q}_{\mathfrak{e}\varsigma},\ \mathcal{S}_\mathfrak{j} < \mathfrak{i}\mathcal{S}_\varsigma,$$
$$\mathcal{T}_{1\mathfrak{j}} < \mathfrak{i}\mathcal{T}_{1\varsigma},\ \mathcal{T}_{2\mathfrak{j}} < \mathfrak{i}\mathcal{T}_{2\varsigma},\ \mathfrak{i} > 1, \forall\, \mathfrak{j}, \varsigma \in \mathcal{M}, \mathfrak{j} \neq \varsigma, \tag{11}$$

where

$\Xi_1^{\mathfrak{d}\nu} = \Xi_{11}^{\mathfrak{d}\nu} + \Xi_{12}^{\mathfrak{d}\nu}$, $\Xi_{11}^{\mathfrak{d}\nu} = \tilde{\Xi}_{01}^{\mathfrak{d}\nu} + \tilde{\Xi}_{02}^{\mathfrak{d}\nu} + \tilde{\Xi}_{03}^{\mathfrak{d}\nu} + \tilde{\Xi}_{04}^{\mathfrak{d}\nu} + \tilde{\Xi}_{05}^{\mathfrak{d}\nu} + \tilde{\Xi}_{06}^{\mathfrak{d}\nu}$,

$\tilde{\Xi}_{01}^{\mathfrak{d}\nu} = sym\{\Phi_1^T\mathcal{P}_{1\mathfrak{j}}\Phi_8 - \Psi_3^T\mathcal{Q}_{2\mathfrak{j}}\Psi_4 + \gamma\Phi_1^T\mathcal{P}_{1\mathfrak{j}}\Phi_1\}$, $\tilde{\Xi}_{02}^{\mathfrak{d}\nu} = sym\{\mathcal{W}_a^T\Psi_5 - 2\mathcal{W}_b^T\Phi_6\}$, $\tilde{\Xi}_{03}^{\mathfrak{d}\nu} = sym\{-\mathcal{V}_a^T\Psi_7 - 2\mathcal{V}_b^T\Phi_7\}$, $\tilde{\Xi}_{04}^{\mathfrak{d}\nu} = \Psi_1^T\mathcal{P}_{2\mathfrak{j}}\Psi_1 + \Psi_2^T\mathcal{P}_{3\mathfrak{j}}\Psi_2$, $\tilde{\Xi}_{05}^{\mathfrak{d}\nu} = \bar{\imath}^2\Phi_1^T\mathcal{P}_{4\mathfrak{j}}\Phi_1 + \Psi_3^T\mathcal{Q}_{1\mathfrak{j}}\Psi_3$, $\tilde{\Xi}_{06}^{\mathfrak{d}\nu} = \Psi_{10}^T\mathcal{Q}_{3\mathfrak{j}}\Psi_{10} + \Psi_{10}^T\mathcal{Q}_{4\mathfrak{j}}\Psi_4$,

$\Xi_{12}^{\mathfrak{d}\nu} = sym\{\hat{\Xi}_{01}^{\mathfrak{d}\nu}\hat{\Xi}_{02}^{\mathfrak{d}\nu}\} + \hat{\Xi}_{03}^{\mathfrak{d}\nu} + \hat{\Xi}_{04}^{\mathfrak{d}\nu} + \hat{\Xi}_{05}^{\mathfrak{d}\nu}$, $\hat{\Xi}_{01}^{\mathfrak{d}\nu} = \Phi_1^T\mathcal{Z}_{1\mathfrak{j}} + \Phi_8^T\wp\mathcal{Z}_{1\mathfrak{j}}$,

$\hat{\Xi}_{02}^{\mathfrak{d}\nu} = \tilde{\mathfrak{A}}_{\mathfrak{j}\mathfrak{d}}\Phi_1 + \tilde{\mathfrak{V}}_{\mathfrak{j}\mathfrak{d}}\Phi_2 + \bar{\beta}\tilde{\mathfrak{B}}_{\mathfrak{j}\mathfrak{d}}\{\bar{\alpha}\tilde{\mathfrak{H}}_{\mathfrak{j}\nu}\Phi_9 + (1-\bar{\alpha})\tilde{\mathfrak{H}}_{\mathfrak{j}\nu}\Phi_4\} + \tilde{\mathfrak{D}}_{\mathfrak{j}\mathfrak{d}}\Phi_{10} - \Phi_8$,

$\hat{\Xi}_{03}^{\mathfrak{d}\nu} = -\Phi_{10}^T\mathcal{U}\Phi_{10} + \Phi_4^T\mathcal{F}^T\mathcal{E}\mathcal{F}\Phi_4 - \Phi_9^T\mathcal{E}\Phi_9$,

$\hat{\Xi}_{04}^{\mathfrak{d}\nu} = -\Phi_{11}^T(9\mathcal{P}_{4\mathfrak{j}})\Phi_{11} + \Phi_{11}^T\big(\frac{36}{\imath}\mathcal{P}_{4\mathfrak{j}}\big)\Phi_{12} - \Phi_{11}^T\big(\frac{60}{\imath^2}\mathcal{P}_{4\mathfrak{j}}\big)\Phi_{13}$,
$\hat{\Xi}_{05}^{\mathfrak{d}\nu} = -\Phi_{12}^T\big(\frac{192}{\imath^2}\mathcal{P}_{4\mathfrak{j}}\big)\Phi_{12} + \Phi_{12}^T\big(\frac{360}{\imath^3}\mathcal{P}_{4\mathfrak{j}}\big)\Phi_{13} - \Phi_{13}^T\big(\frac{720}{\imath^4}\mathcal{P}_{4\mathfrak{j}}\big)\Phi_{13}$,

$\Xi_2^{\mathfrak{d}\nu} = sym\{\Psi_3^T\mathcal{Q}_{1\mathfrak{j}}\Psi_9 + \Psi_9^T\mathcal{Q}_{2\mathfrak{j}}\Psi_4 + \mathcal{V}_b^T\Psi_8\} + \Psi_4^T\mathcal{S}_\mathfrak{j}\Psi_4 + \Phi_8^T\mathcal{T}_{1\mathfrak{j}}\Phi_8$,

$\Xi_3^{\mathfrak{d}\nu} = sym\{\Psi_{10}^T\mathcal{Q}_{3\mathfrak{j}}\Psi_{11} + \Psi_{11}^T\mathcal{Q}_{4\mathfrak{j}}\Psi_4 + \mathcal{W}_b^T\Psi_6\} - \Psi_4^T\mathcal{S}_\mathfrak{j}\Psi_4 + \Phi_8^T\mathcal{T}_{2\mathfrak{j}}\Phi_8$,

$\Psi_1 = \Phi_1 - \Phi_3$, $\Psi_2 = \Phi_1 - (1-\kappa)\Phi_2$, $\Psi_3 = col\{\Phi_1 - \Phi_4,\ \Phi_6\}$, $\Psi_4 = col\{\Phi_4,\ \Phi_5\}$, $\Psi_5 = \Phi_1 - \Phi_4$, $\Psi_6 = \Phi_1 + \Phi_4$, $\Psi_7 = \Phi_1 - \Phi_5$, $\Psi_8 = \Phi_1 + \Phi_5$, $\Psi_9 = col\{\Phi_8,\ \Phi_1\}$, $\Psi_{10} = col\{\Phi_1 - \Phi_5,\ \Phi_7\}$, $\Psi_{11} = col\{\Phi_8,\ -\Phi_1\}$, $\hat{\mathcal{P}}_{\mathfrak{e}\mathfrak{j}} = \mathcal{D}^{-\frac{1}{2}}\mathcal{P}_{\mathfrak{e}\mathfrak{j}}\mathcal{D}^{-\frac{1}{2}}$, $\phi_1 = \phi_{min}(\hat{\mathcal{P}}_{1\mathfrak{j}})$, $\phi_2 = \phi_{max}(\hat{\mathcal{P}}_{1\mathfrak{j}})$, $\phi_3 = \phi_{max}(\hat{\mathcal{P}}_{2\mathfrak{j}})$, $\phi_4 = \phi_{max}(\hat{\mathcal{P}}_{3\mathfrak{j}})$, $\phi_5 = \phi_{max}(\hat{\mathcal{P}}_{4\mathfrak{j}})$, $\mathcal{Z}_{2\mathfrak{j}} = \wp\mathcal{Z}_{1\mathfrak{j}}$.

$$\bar{\phi}C_1 + \delta_b[e^{\gamma\mathcal{G}_\mathfrak{w}} - 1] < e^{\gamma\mathcal{G}_\mathfrak{w}}\phi_1 C_2. \tag{12}$$

Further, when $\imath > 1$, the average dwell time obeys

$$\varkappa > \varkappa^* = \frac{\mathcal{G}_\mathfrak{f} ln\imath}{ln(\phi_1 C_2) - ln\big(\bar{\phi}C_1 + \delta_b[e^{\gamma\mathcal{G}_\mathfrak{w}} - 1]\big) + \gamma\mathcal{G}_\mathfrak{f}}. \tag{13}$$

Proof. To substantiate the foregoing assertion, we harness Lyapunov stability theory. In this circumstance, we put forward a looped-type Lyapunov functional in the following manner:

$$\mathfrak{Q}(t) = \mathfrak{Q}_0(t) + \mathfrak{Q}_a(t), \tag{14}$$

where $\mathfrak{Q}_0(t)$ is Lyapunov functional designated as $\mathfrak{Q}_0(t) = \hat{\mathfrak{Q}}_0(t) + \tilde{\mathfrak{Q}}_0(t)$ and $\mathfrak{Q}_a(t)$ is a two-sided looped-functional which is defined as $\mathfrak{Q}_a(t) = \mathfrak{Q}_1(t) + \mathfrak{Q}_2(t) + \mathfrak{Q}_3(t)$.

$\hat{\mathfrak{Q}}_0(t) = \vartheta^T(t)\mathcal{P}_{1\mathfrak{j}}\vartheta(t)$,

$\tilde{\mathfrak{Q}}_0(t) = \int_{t-\bar{\imath}}^{t}\vartheta^T(s)\mathcal{P}_{2\mathfrak{j}}\vartheta(s)ds + \int_{t-\imath(t)}^{t}\vartheta^T(s)\mathcal{P}_{3\mathfrak{j}}\vartheta(s)ds + \bar{\imath}\int_{-\bar{\imath}}^{0}\int_{t+s}^{t}\vartheta^T(r)\mathcal{P}_{4\mathfrak{j}}\vartheta(r)drds$,

$\mathfrak{Q}_1(t) = (t_{\mathfrak{k}+1} - t)\aleph_1^T(t)\big[\mathcal{Q}_{1\mathfrak{j}}\aleph_1(t) + 2\mathcal{Q}_{2\mathfrak{j}}\aleph_3(t)\big] + (t - t_\mathfrak{k})\aleph_2^T(t)\big[\mathcal{Q}_{3\mathfrak{j}}\aleph_2(t) + 2\mathcal{Q}_{4\mathfrak{j}}\aleph_3(t)\big]$,

$\mathfrak{Q}_2(t) = (\mathfrak{t}_{\mathfrak{k}+1} - t)(t - t_\mathfrak{k})\aleph_3^T(t)\mathcal{S}_\mathfrak{j}\aleph_3(t)$,

$\mathfrak{Q}_3(t) = (t_{\mathfrak{k}+1} - t)\int_{t_\mathfrak{k}}^{t}\vartheta^T(s)\mathcal{T}_{1\mathfrak{j}}\vartheta(s)ds - (t - t_\mathfrak{k})\int_{t}^{t_{\mathfrak{k}+1}}\vartheta^T(s)\mathcal{T}_{2\mathfrak{j}}\vartheta(s)ds$.

Subsequently, we can infer the resultant set of connection through utilizing the mathematical expectation on each side of Eq. (14), together with the solution route pertaining to relations (8).

$$\mathbb{E}\{\dot{\hat{\mathfrak{Q}}}_0(t)\} = \mathbb{E}\big\{2\vartheta^T(t)\mathcal{P}_{1\mathfrak{j}}\dot{\vartheta}(t)\big\}, \tag{15}$$

$$\mathbb{E}\{\dot{\tilde{\mathfrak{Q}}}_0(t)\} \leq \mathbb{E}\Big\{\vartheta^T(t)\mathcal{P}_{2\mathfrak{j}}\vartheta(t) - \vartheta^T(t-\bar{\imath})\mathcal{P}_{2\mathfrak{j}}\vartheta(t-\bar{\imath}) + \vartheta^T(t)\mathcal{P}_{3\mathfrak{j}}\vartheta(t) - (1-\kappa)$$
$$\vartheta^T(t-\imath(t))\mathcal{P}_{3\mathfrak{j}}\vartheta(t-\imath(t)) + \bar{\imath}^2\vartheta^T(t)\mathcal{P}_{4\mathfrak{j}}\vartheta(t) - \bar{\imath}\int_{t-\bar{\imath}}^{t}\vartheta^T(s)\mathcal{P}_{4\mathfrak{j}}\vartheta(s)ds\Big\}. \tag{16}$$

$$\mathbb{E}\{\dot{\Omega}_1(t)\} = \mathbb{E}\Big\{\aleph_1^T\big[-\mathcal{Q}_{1\mathrm{j}}\aleph(t) - 2\mathcal{Q}_{2\mathrm{j}}\aleph_3(t)\big] + (t_{\mathfrak{k}+1}-t)\aleph_1^T(t)\mathcal{Q}_{1\mathrm{j}}\dot{\aleph}_1(t) + 2(t_{\mathfrak{k}+1}-t)\dot{\aleph}_1(t)\mathcal{Q}_{2\mathrm{j}}\aleph_3(t) + \aleph_2^T(t)\mathcal{Q}_{3\mathrm{j}}\aleph_2(t) + (t-t_{\mathfrak{k}+1})\aleph_2^T(t)\mathcal{Q}_{3\mathrm{j}}\dot{\aleph}_2(t) + \aleph_2^T(t)\mathcal{Q}_{3\mathrm{j}}\aleph_3(t) + 2(t-t_{\mathfrak{k}+1})\dot{\aleph}_2^T(t)\mathcal{Q}_{4\mathrm{j}}\aleph_3(t)\Big\}, \tag{17}$$

$$\mathbb{E}\{\dot{\Omega}_2(t)\} = \mathbb{E}\Big\{-(t-t_{\mathfrak{k}})\aleph_3^T(t)S_{\mathrm{j}}\aleph_3(t) + (t_{\mathfrak{k}+1}-t)\aleph_3^T(t)S_{\mathrm{j}}\aleph_3(t)\Big\}, \tag{18}$$

$$\mathbb{E}\{\dot{\Omega}_3(t)\} = \mathbb{E}\Big\{(t_{\mathfrak{k}+1}-t)\dot{\vartheta}^T(t)\mathcal{T}_{1\mathrm{j}}\dot{\vartheta}(t) + (t-t_{\mathfrak{k}})\dot{\vartheta}^T(t)\mathcal{T}_{2\mathrm{j}}\dot{\vartheta}(t) - \int_{t_{\mathfrak{k}}}^{t}\dot{\vartheta}^T(s)\mathcal{T}_{1\mathrm{j}}\dot{\vartheta}(s)ds - \int_{t}^{t_{\mathfrak{k}+1}}\dot{\vartheta}^T(s)\mathcal{T}_{2\mathrm{j}}\dot{\vartheta}(s)ds\Big\}. \tag{19}$$

Subsequently, with the support of Lemma 1 and 2, the integral inequalities can be reformulated as in the following framework:

$$-\bar{\imath}\int_{t-\bar{\imath}}^{t}\vartheta^T(s)\mathcal{P}_{4\mathrm{j}}\vartheta(s)ds \le \daleth^T(t)\begin{bmatrix}-9\mathcal{P}_{4\mathrm{j}} & \frac{36}{\bar{\imath}}\mathcal{P}_{4\mathrm{j}} & -\frac{60}{\bar{\imath}^2}\mathcal{P}_{4\mathrm{j}}\\ * & -\frac{192}{\bar{\imath}^2}\mathcal{P}_{4\mathrm{j}} & \frac{360}{\bar{\imath}^3}\mathcal{P}_{4\mathrm{j}}\\ * & * & -\frac{720}{\bar{\imath}^4}\mathcal{P}_{4\mathrm{j}}\end{bmatrix}\daleth(t), \tag{20}$$

$$-\int_{t_{\mathfrak{k}}}^{t}\dot{\vartheta}^T(s)\mathcal{T}_{1j}\dot{\vartheta}(s)ds \le \theta^T(t)\Omega_1\theta(t), \tag{21}$$

$$-\int_{t}^{t_{\mathfrak{k}+1}}\dot{\vartheta}^T(s)\mathcal{T}_{2j}\dot{\vartheta}(s)ds \le \theta^T(t)\Omega_2\theta(t), \tag{22}$$

where

$$\daleth(t) = \left[\int_{t-\bar{\imath}}^{t}\vartheta^T(s)ds \int_{t-\bar{\imath}}^{t}\int_{t-\bar{\imath}}^{s}\vartheta^T(v)dvds \int_{-\bar{\imath}}^{0}\int_{t-\bar{\imath}}^{t+s}\int_{t-\bar{\imath}}^{t+v}\vartheta^T(w)dwdvds\right]^T,$$

$$\Omega_1 = (t-t_{\mathfrak{k}})\big[\mathcal{W}_a^T\mathcal{T}_{1j}^{-1}\mathcal{W}_a + \frac{\eta_2^2}{3}\mathcal{W}_b^T\mathcal{T}_{1j}^{-1}\mathcal{W}_b\big] + sym\big\{\mathcal{W}_a^T\Psi_6 - 2\mathcal{W}_b^T\Phi_6 + (t-t_{\mathfrak{k}})\mathcal{W}_b^T\Psi_7\big\},$$

$$\Omega_2 = (t_{\mathfrak{k}+1}-t)[\mathcal{V}_a^T\mathcal{T}_{2j}^{-1}\mathcal{V}_a + \frac{\eta_2^2}{3}\mathcal{V}_b^T\mathcal{T}_{2j}^{-1}\mathcal{V}_b] + sym\big\{\mathcal{V}_a^T\Psi_8 - 2\mathcal{V}_b^T\Phi_7 + (t_{\mathfrak{k}+1}-t)\mathcal{V}_b^T\Psi_9\big\}.$$

Then, through the utilization of Assumption 2, we have established the ensuing connection for matrix $\mathcal{E} > 0$:

$$\vartheta^T(t_{\mathfrak{k}})\mathcal{F}^T\mathcal{E}\mathcal{F}\vartheta(t_{\mathfrak{k}}) - \mathfrak{f}^T(\vartheta(t_{\mathfrak{k}}))\mathcal{E}\mathfrak{f}(\vartheta(t_{\mathfrak{k}})) \ge 0. \tag{23}$$

Moreover, for any matrices $\mathcal{Z}_{1\mathrm{j}}$ and $\mathcal{Z}_{2\mathrm{j}}$, it is easy to deduce the following connection:

$$2\big[\vartheta^T(t)\mathcal{Z}_{1\mathrm{j}} + \dot{\vartheta}^T(t)\mathcal{Z}_{2\mathrm{j}}\big]\big[\tilde{\mathfrak{A}}_{\mathrm{j}\mathfrak{d}}\vartheta(t) + \tilde{\mathfrak{V}}_{\mathrm{j}\mathfrak{d}}\vartheta(t-\imath(t)) + \tilde{\mathfrak{B}}_{\mathrm{j}\mathfrak{d}}\beta(t)\{\mathfrak{H}_{\mathrm{j}\nu}\alpha(t)\mathfrak{f}(\vartheta(t_{\mathfrak{k}})) + (1-\alpha(t))\mathfrak{H}_{\mathrm{j}\nu}\vartheta(t_{\mathfrak{k}})\} + \tilde{\mathfrak{D}}_{\mathrm{j}\mathfrak{d}}\delta(t) - \dot{\delta}(t)\big] = 0. \tag{24}$$

Based on the foregoing setting, by accumulating the Eqs. (15)–(24), the ensuing constraints can be established for $t \in [t_{\mathfrak{k}}, t_{\mathfrak{k}+1})$.

$$\mathbb{E}\big\{\dot{\mathfrak{V}}(t) + \gamma\mathfrak{V}(t) - \delta^T(t)\mathcal{U}\delta(t)\big\} \le \sum_{\mathfrak{d}=1}^{\mathfrak{q}}\sum_{\nu=1}^{\mathfrak{q}}\mathfrak{h}_{\mathrm{j}\mathfrak{d}}(\mathfrak{E}(t))\mathfrak{h}_{\mathrm{j}\nu}(\mathfrak{E}(t))\theta^T(t) \times\left[\frac{t_{\mathfrak{k}+1}-t}{\mathfrak{y}_{\mathfrak{k}}}\Delta_1^{\mathfrak{d}\nu} + \frac{t-t_{\mathfrak{k}}}{\mathfrak{y}_{\mathfrak{k}}}\Delta_2^{\mathfrak{d}\nu}\right]\theta(t), \tag{25}$$

where

$$\Delta_1^{\mathfrak{d}\nu} = \Xi_1^{\mathfrak{d}\nu} + \mathfrak{y}_{\mathfrak{k}}\left[\mathcal{V}_a^T\mathcal{T}_{2j}^{-1}\mathcal{V}_a + \frac{\eta_2^2}{3}\mathcal{V}_b^T\mathcal{T}_{2j}^{-1}\mathcal{V}_b\right],$$

$$\Delta_2^{\mathfrak{d}\nu} = \Xi_1^{\mathfrak{d}\nu} + \mathfrak{y}_{\mathfrak{k}}\left[\mathcal{W}_a^T\mathcal{T}_{1j}^{-1}\mathcal{W}_a + \frac{\eta_2^2}{3}\mathcal{W}_b^T\mathcal{T}_{1j}^{-1}\mathcal{W}_b\right].$$

In this setting, the statement of theorem offers the elements of $\Xi_1^{\mathfrak{d}\nu}$ and by deploying the Schur complement lemma [36], the above-given matrices $\Delta_1^{\mathfrak{d}\nu}$ and $\Delta_2^{\mathfrak{d}\nu}$ can be transformed into the matrices in the theorem.

Subsequently, if the constraints (9) and (10) hold, then the below-given inequality can be obtained effortlessly.

$$\mathbb{E}\big\{\dot{\mathfrak{V}}(t) + \gamma\mathfrak{V}(t) - \delta^T(t)\mathcal{U}\delta(t)\big\} \le 0. \tag{26}$$

Thereafter, integrating the above relation from $t_{\mathfrak{k}}$ to t and based on Assumption 1, we can procure the following results:

$$\mathbb{E}\big\{\mathfrak{V}(t)\big\} \le e^{-\gamma(t-t_{\mathfrak{k}})}\Big[\mathbb{E}\{\mathfrak{V}(t_{\mathfrak{k}})\} + \delta_b[e^{\gamma(t-t_k)} - 1]\Big]. \tag{27}$$

In light of (11), we establish the below-offered relation:

$$\mathbb{E}\big\{\mathfrak{V}(t_{\mathfrak{k}})\big\} \le \mathfrak{i}\mathbb{E}\big\{\mathfrak{V}(t_{\mathfrak{k}}^-)\big\}, \text{ where } \mathfrak{i} > 1. \tag{28}$$

Subsequently, based on (27) and (28), we can arrive at the following inequalities:

$$\begin{aligned}\mathbb{E}\big\{\mathfrak{V}(t)\big\} &< \mathfrak{i}e^{-\gamma(t-t_{\mathfrak{k}})}\mathbb{E}\big\{\mathfrak{V}(t_{\mathfrak{k}}^-) + \delta_b[e^{-\gamma(t-t_{\mathfrak{k}})} - 1]\big\}\\ &< \mathfrak{i}^2e^{-\gamma(t-t_{\mathfrak{k}-1})}\mathbb{E}\big\{\mathfrak{V}(t_{\mathfrak{k}}^-) + \delta_b[e^{\gamma(t-t_{\mathfrak{k}-1})} - 1]\big\}\\ &< \ldots < \mathfrak{i}^{\mathcal{N}_{\mathrm{j}}(0,\mathcal{G}_{\mathfrak{w}})}e^{-\gamma\mathcal{G}_{\mathfrak{w}}}\mathbb{E}\big\{\mathfrak{V}(0) + \delta_b[e^{\gamma\mathcal{G}_{\mathfrak{w}}} - 1]\big\},\end{aligned} \tag{29}$$

here $\mathcal{N}_{\mathrm{j}}(0,\mathcal{G}_{\mathfrak{w}}) < \frac{\mathcal{G}_{\mathfrak{w}}}{\varkappa}$ represents the number of switchings in the j-th subsystem.

Next, let us consider the connection $\hat{\mathcal{P}}_{\mathfrak{e}\mathrm{j}} = \mathcal{D}^{-\frac{1}{2}}\mathcal{P}_{\mathfrak{e}\mathrm{j}}\mathcal{D}^{-\frac{1}{2}}$ for any symmetric matrix $\mathcal{D}$ and by using this connection, we yield the following relation:

$$\mathbb{E}\big\{\mathfrak{V}(t)\big\} \ge \mathbb{E}\{\vartheta^T(t)\mathcal{P}_{1\mathrm{j}}\vartheta(t)\} \ge \phi_{min}(\hat{\mathcal{P}}_{1\mathrm{j}})\mathbb{E}\{\vartheta^T(t)\mathcal{D}\vartheta(t)\} = \phi_1\mathbb{E}\{\vartheta^T(t)\mathcal{D}\vartheta(t)\}. \tag{30}$$

In turn, under the zero initial constraint, we procure the following connection:

$$\begin{aligned}\mathbb{E}\big\{\mathfrak{V}(0)\big\} &= \vartheta^T(0)\mathcal{P}_{1\mathrm{j}}\vartheta(0) + \int_{-\bar{\imath}}^{0}\vartheta^T(s)\mathcal{P}_{2\mathrm{j}}\vartheta(s)ds + \int_{-\imath(0)}^{0}\vartheta^T(s)\mathcal{P}_{3\mathrm{j}}\vartheta(s)ds + \bar{\imath}\int_{-\bar{\imath}}^{0}\int_{s}^{0}\vartheta^T(r)\mathcal{P}_{4\mathrm{j}}\vartheta(r)drds\\ &\le \left[\phi_{max}(\hat{\mathcal{P}}_{1\mathrm{j}}) + \bar{\imath}\phi_{max}(\hat{\mathcal{P}}_{2\mathrm{j}}) + \bar{\imath}\phi_{max}(\hat{\mathcal{P}}_{3\mathrm{j}}) + \frac{\bar{\imath}^3}{2}\phi_{max}(\hat{\mathcal{P}}_{4\mathrm{j}})\right]\sup_{-\bar{\imath}\le t_0<0}\mathbb{E}\{\vartheta^T(t_0)\mathcal{D}\vartheta(t_0)\}\\ &= [\phi_2 + \bar{\imath}\phi_3 + \bar{\imath}\phi_4 + \frac{\bar{\imath}^3}{2}\phi_5]\mathcal{C}_1\\ &= \bar{\phi}\mathcal{C}_1.\end{aligned} \tag{31}$$

Thereafter, with the amalgamation of (29)–(31), we obtain the following criteria:

$$\phi_1\mathbb{E}\{\vartheta^T(t)\mathcal{D}\vartheta(t)\} \le \mathfrak{i}^{\frac{\mathcal{G}_{\mathfrak{w}}}{\varkappa}}e^{-\gamma\mathcal{G}_{\mathfrak{f}}}[\bar{\phi}\mathcal{C}_1 + \delta_b[e^{\gamma\mathcal{G}_{\mathfrak{w}}} - 1]]. \tag{32}$$

Then, if constraints (12) and (13) in the statement of the theorem hold, we can derive the following inequality:

$$\mathbb{E}\{\vartheta^T(t)\mathcal{D}\vartheta(t)\} < \mathcal{C}_2. \tag{33}$$

After this, in light of Definition 1, it is straightforward to arrive at the statement that the system (8) is finite-time bounded with respect to $(\mathcal{C}_1, \mathcal{C}_2, \mathcal{G}_{\mathfrak{w}}, \gamma, \mathcal{D})$, which concludes the proof of this theorem. □

3.2. Finite-time bounded and extended dissipative investigation

Theorem 2. *For the stated scalars $\bar{\imath}, \kappa, \mathfrak{y}_1, \mathfrak{y}_2, \bar{\alpha}, \bar{\beta}, \wp$, known gain matrices of the controller $\tilde{\mathfrak{H}}_{\mathfrak{j}\nu}$ and under the Assumptions 1–5, if there exist positive definite matrices $\mathcal{P}_{\mathfrak{e}\mathfrak{j}}$, $\mathcal{T}_{1\mathfrak{j}}$ and $\mathcal{T}_{2\mathfrak{j}}$, matrices $\mathcal{Q}_{\mathfrak{e}\mathfrak{j}}$ ($\mathfrak{e} = 1, 2, 3, 4$), $\mathcal{S}_{\mathfrak{j}}$, then the closed-loop system (8) is said to be finite-time bounded with respect to $(C_1, C_2, \mathcal{G}_{\mathfrak{w}}, \gamma, D)$ and extended dissipative, such that the following conditions hold:*

$$\begin{bmatrix} \tilde{\Xi}_1^{\mathfrak{d}\nu} + \mathfrak{y}_{\mathfrak{k}}\Xi_2^{\mathfrak{d}\nu} & \sqrt{\mathfrak{y}_{\mathfrak{k}}}\mathcal{V}_a^T & \sqrt{\mathfrak{y}_{\mathfrak{k}}}\mathfrak{y}_2\mathcal{V}_b^T \\ * & -\mathcal{T}_{2j} & 0 \\ * & * & -3\mathcal{T}_{2j} \end{bmatrix} < 0, \tag{34}$$

$$\begin{bmatrix} \tilde{\Xi}_1^{\mathfrak{d}\nu} + \mathfrak{y}_{\mathfrak{k}}\Xi_3^{\mathfrak{d}\nu} & \sqrt{\mathfrak{y}_{\mathfrak{k}}}\mathcal{W}_a^T & \sqrt{\mathfrak{y}_{\mathfrak{k}}}\mathfrak{y}_2\mathcal{W}_b^T \\ * & -\mathcal{T}_{1j} & 0 \\ * & * & -3\mathcal{T}_{1j} \end{bmatrix} < 0, \tag{35}$$

$$\begin{aligned} &\mathcal{P}_{\mathfrak{e}\mathfrak{j}} < \mathrm{i}\mathcal{P}_{\mathfrak{e}\varsigma},\ \mathcal{Q}_{\mathfrak{e}\mathfrak{j}} < \mathrm{i}\mathcal{Q}_{\mathfrak{e}\varsigma},\ \mathcal{S}_{\mathfrak{j}} < \mathrm{i}\mathcal{S}_{\varsigma}, \\ &\mathcal{T}_{1\mathfrak{j}} < \mathrm{i}\mathcal{T}_{1\varsigma},\ \mathcal{T}_{2\mathfrak{j}} < \mathrm{i}\mathcal{T}_{2\varsigma}, \mathrm{i} > 1, \forall\, \mathfrak{j}, \varsigma \in \mathcal{M}, \mathfrak{j} \neq \varsigma, \end{aligned} \tag{36}$$

$$\frac{1}{\mathsf{a}}\mathcal{P}_{1\mathfrak{j}} - \tilde{\mathfrak{C}}_{\mathfrak{j}\mathfrak{d}}F_4\tilde{\mathfrak{C}}_{\mathfrak{j}\mathfrak{d}} > 0, \tag{37}$$

the average dwell time satisfies

$$\varkappa > \varkappa^* = \frac{\mathcal{G}_{\mathfrak{f}} ln\imath}{ln(\phi_1 C_2) - ln\big(\phi_6 \mathsf{k} + (\phi_7 + \phi_8)\delta_b\big) + \gamma\mathcal{G}_{\mathfrak{w}}}, \tag{38}$$

where

$\tilde{\Xi}_1^{\mathfrak{d}\nu} = \Xi_{11}^{\mathfrak{d}\nu} + \Omega_{12}^{\mathfrak{d}\nu}$, $\Omega_{12}^{\mathfrak{d}\nu} = sym\{\hat{\Xi}_{01}^{\mathfrak{d}\nu}\hat{\Xi}_{02}^{\mathfrak{d}\nu} - \hat{\Omega}_{01}^{\mathfrak{d}\nu}\} + \hat{\Omega}_{02}^{\mathfrak{d}\nu} + \hat{\Xi}_{04}^{\mathfrak{d}\nu} + \hat{\Xi}_{05}^{\mathfrak{d}\nu}$,
$\hat{\Omega}_{01}^{\mathfrak{d}\nu} = \Phi_1^T F_2\Phi_{10}$, $\hat{\Omega}_{02}^{\mathfrak{d}\nu} = -\Phi_1^T\tilde{\mathfrak{C}}_{\mathfrak{j}\mathfrak{d}}^T F_1\tilde{\mathfrak{C}}_{\mathfrak{j}\mathfrak{d}}\Phi_1 - \Phi_{10}^T F_3\Phi_{10} + \Phi_4^T\mathcal{F}^T\mathcal{E}\mathcal{F}\Phi_4 - \Phi_9^T\mathcal{E}\Phi_9$, $\phi_6 = \phi_{max}(\tilde{\mathfrak{C}}_{\mathfrak{j}\mathfrak{d}}^T\tilde{\mathfrak{C}}_{\mathfrak{j}\mathfrak{d}})$, $\phi_7 = \phi_{max}(F_2^T F_2)$, $\phi_8 = \phi_{max}(F_3)$.

Proof. In order to prove this argument, we formulate the same Lyapunov functional (14) which is offered in the former theorem. Subsequently, by following similar lines of the previous theorem and by implementing the extended dissipative $\mathcal{H}(t)$, we can directly obtain the following connection:

$$\begin{aligned} \mathbb{E}\{\dot{\mathfrak{Q}}(t) + \gamma\mathfrak{Q}(t) - \mathcal{H}(t)\} \leq \sum_{\mathfrak{d}=1}^{\mathfrak{q}}\sum_{\nu=1}^{\mathfrak{q}} \mathfrak{h}_{\mathfrak{j}\mathfrak{d}}(\mathfrak{E}(t))\mathfrak{h}_{\mathfrak{j}\nu}(\mathfrak{E}(t))\theta^T(t) \\ \times\left[\frac{t_{\mathfrak{k}+1} - t}{\mathfrak{y}_{\mathfrak{k}}}\bar{\Delta}_1^{\mathfrak{d}\nu} + \frac{t - t_{\mathfrak{k}}}{\mathfrak{y}_{\mathfrak{k}}}\bar{\Delta}_2^{\mathfrak{d}\nu}\right]\theta(t), \end{aligned} \tag{39}$$

where

$$\begin{aligned} \bar{\Delta}_1^{\mathfrak{d}\nu} &= \tilde{\Xi}_1^{\mathfrak{d}\nu} + \mathfrak{y}_{\mathfrak{k}}\left[\mathcal{V}_a^T\mathcal{T}_{2j}^{-1}\mathcal{V}_a + \frac{\mathfrak{y}_2^2}{3}\mathcal{V}_b^T\mathcal{T}_{2j}^{-1}\mathcal{V}_b\right], \\ \bar{\Delta}_2^{\mathfrak{d}\nu} &= \tilde{\Xi}_1^{\mathfrak{d}\nu} + \mathfrak{y}_{\mathfrak{k}}\left[\mathcal{W}_a^T\mathcal{T}_{1j}^{-1}\mathcal{W}_a + \frac{\mathfrak{y}_2^2}{3}\mathcal{W}_b^T\mathcal{T}_{1j}^{-1}\mathcal{W}_b\right]. \end{aligned}$$

Further, by tracing the similar fashion of the previous theorem, from (34), (35), we derive

$$\mathbb{E}\{\dot{\mathfrak{Q}}(t) + \gamma\mathfrak{Q}(t) - \mathcal{H}(t)\} < 0. \tag{40}$$

Thereafter, in light of the inequality (29), we establish

$$\mathbb{E}\{\mathfrak{Q}(t)\} < \mathbb{E}\left\{\mathrm{i}^{\mathcal{N}_{\mathfrak{j}}(0,t)}e^{-\gamma t}\mathfrak{Q}(0) + \int_0^t \mathrm{i}^{\mathcal{N}_{\mathfrak{j}}(s,t)}e^{-\gamma(t-s)}\mathcal{H}(s)ds\right\}. \tag{41}$$

In the context of zero initial constraints, we obtain the following relation:

$$\mathbb{E}\{\mathfrak{Q}(t)\} < \mathbb{E}\left\{\mathrm{i}^{\mathcal{N}_{\mathfrak{j}}(0,t)}e^{-\gamma t}\int_0^t \mathcal{H}(s)ds\right\}. \tag{42}$$

The above equation can be reframed as

$$\mathbb{E}\left\{\frac{\mathfrak{Q}(t)}{\mathrm{i}^{\mathcal{N}_{\mathfrak{j}}(0,t)}e^{-\gamma t}}\right\} < \mathbb{E}\left\{\int_0^t \mathcal{H}(s)ds\right\}. \tag{43}$$

With the help of Assumption 5, we attain

$$\mathbb{E}\left\{\frac{\mathfrak{Q}(t)}{\mathsf{a}}\right\} < \mathbb{E}\left\{\int_0^t \mathcal{H}(s)ds\right\}. \tag{44}$$

Then, we obtain

$$\mathbb{E}\left\{\int_0^t \mathcal{H}(s)ds\right\} > \mathbb{E}\left\{\frac{\mathfrak{Q}(t)}{\mathsf{a}}\right\} > \frac{1}{\mathsf{a}}\mathbb{E}\{\vartheta^T(t)\mathcal{P}_{1\mathfrak{j}}\vartheta(t)\} > 0. \tag{45}$$

Further, let us consider the connection

$$\mathbb{E}\left\{\int_0^{\mathcal{G}_{\mathfrak{w}}} \mathcal{H}(s)ds - \sup_{0\leq t\leq\mathcal{G}_{\mathfrak{w}}} \xi^T(t)F_4\xi(t)\right\} \geq 0. \tag{46}$$

Next, in accordance with the Assumption 4, we have two cases, namely, $F_4 = 0$ and $F_4 > 0$.

Case (I): When $F_4 = 0$, we directly compute

$$\mathbb{E}\left\{\int_0^{\mathcal{G}_{\mathfrak{w}}} \mathcal{H}(s)ds\right\} \geq 0. \tag{47}$$

Then the above system can be deduced to the H_∞, passivity and dissipativity performances.

Case (II): When $F_4 > 0$, based on Assumption 4, we have $F_1 = 0$, $F_2 = 0$ and $F_3 > 0$, we attain

$$\mathbb{E}\left\{\int_0^{\mathcal{G}_{\mathfrak{w}}} \mathcal{H}(s)ds\right\} > \mathbb{E}\left\{\int_0^{\mathcal{G}_{\mathfrak{w}}} \delta^T(s)F_3\delta(s)ds\right\}. \tag{48}$$

And, for $\forall t \in [0, \mathcal{G}_{\mathfrak{w}}]$, we have

$$\mathbb{E}\left\{\int_0^{\mathcal{G}_{\mathfrak{w}}} \mathcal{H}(s)ds\right\} > \mathbb{E}\left\{\int_0^t \mathcal{H}(s)ds\right\} \geq \frac{1}{\mathsf{a}}\mathbb{E}\{\vartheta^T(t)\mathcal{P}_{1\mathfrak{j}}\vartheta(t)\} > 0. \tag{49}$$

On the basis of the constraint (37), we derive

$$\begin{aligned} \mathbb{E}\left\{\int_0^{\mathcal{G}_{\mathfrak{w}}} \mathcal{H}(s)ds\right\} &\geq \frac{1}{\mathsf{a}}\mathbb{E}\{\vartheta^T(t)\mathcal{P}_{1\mathfrak{j}}\vartheta(t)\} \geq \mathbb{E}\{\vartheta^T(t)\tilde{\mathfrak{C}}_{\mathfrak{j}\mathfrak{d}}F_4\tilde{\mathfrak{C}}_{\mathfrak{j}\mathfrak{d}}\vartheta(t)\} \\ &= \mathbb{E}\left\{\xi^T(t)F_4\xi(t)\right\}. \end{aligned} \tag{50}$$

In this regard, we obtain,

$$\mathbb{E}\left\{\int_0^{\mathcal{G}_{\mathfrak{w}}} \mathcal{H}(s)ds - \sup_{0\leq t\leq\mathcal{G}_{\mathfrak{w}}} \xi^T(t)F_4\xi(t) \geq 0\right\}. \tag{51}$$

Thus, the proof of the extended dissipative segment is completed.

From here, we need to prove the finite-time boundedness of the system. In this connection, from the above argument, we can deduce that

$$\mathbb{E}\{\mathfrak{Q}(t)\} < \mathbb{E}\left\{\mathrm{i}^{\mathcal{N}_{\mathfrak{j}}(0,t)}e^{-\gamma t}\int_0^t \mathcal{H}(s)ds\right\}, \tag{52}$$

$$\mathbb{E}\{\mathfrak{Q}(t)\} < \mathbb{E}\left\{e^{\left(-\gamma + ln\frac{\imath}{\varkappa}\right)\mathcal{G}_{\mathfrak{w}}}\int_0^{\mathcal{G}_{\mathfrak{w}}} \mathcal{H}(s)ds\right\}. \tag{53}$$

When $F_1 \leq 0$, we procure

$$\mathbb{E}\left\{\int_0^{\mathcal{G}_{\mathfrak{w}}} \mathcal{H}(s)ds\right\} \leq \mathbb{E}\left\{\int_0^{\mathcal{G}_{\mathfrak{w}}} \left[2\xi^T(s)F_2\delta(s) + \delta^T(s)F_3\delta(s)\right]ds\right\}, \tag{54}$$

$$\mathbb{E}\{\mathfrak{Q}(t)\} < \mathbb{E}\Big\{ e^{\left(-\gamma+ln\frac{\iota}{\varkappa}\right)\mathcal{G}_{\mathfrak{w}}} \int_0^{\mathcal{G}_{\mathfrak{w}}} \big[2\xi^T(s)F_2\delta(s) + \delta^T(s)F_3\delta(s)\big]ds \Big\}. \quad (55)$$

Then, we obtain

$$\mathbb{E}\{\vartheta^T(t)D\vartheta(t)\} \le \frac{\mathbb{E}\{\mathfrak{Q}(t)\}}{\phi_1} < \mathbb{E}\Big\{ \frac{e^{\left(-\gamma+ln\frac{\iota}{\varkappa}\right)\mathcal{G}_{\mathfrak{w}}}}{\phi_1} \times \int_0^{\mathcal{G}_{\mathfrak{w}}} \big[2\xi^T(s)F_2\delta(s) + \delta^T(s)F_3\delta(s)\big]ds \Big\}. \quad (56)$$

And, with the assist of Lemma 5 in [37], we yield

$$2\xi^T(t)F_2\delta(t) \le \vartheta^T(t)\tilde{\mathfrak{C}}_{\mathfrak{j}\mathfrak{d}}^T\tilde{\mathfrak{C}}_{\mathfrak{j}\mathfrak{d}}\vartheta(t) + \delta^T(t)F_3^TF_3\delta(t). \quad (57)$$

By utilizing the Assumptions 1 and 3, we derive

$$\mathbb{E}\{\vartheta^T(t)D\vartheta(t)\} \le \mathbb{E}\Big\{ \frac{e^{\left(-\gamma+ln\frac{\iota}{\varkappa}\right)\mathcal{G}_{\mathfrak{w}}}}{\phi_1} \int_0^{\mathcal{G}_{\mathfrak{w}}} \big[\vartheta^T(s)\tilde{\mathfrak{C}}_{\mathfrak{j}\mathfrak{d}}^T\tilde{\mathfrak{C}}_{\mathfrak{j}\mathfrak{d}}\vartheta(s) + \delta^T(s)F_2^TF_2\delta(s) + \delta^T(s)F_3^TF_3\delta(s)\big]ds \Big\} \quad (58)$$

$$< \frac{e^{\left(-\gamma+ln\frac{\iota}{\varkappa}\right)\mathcal{G}_{\mathfrak{w}}}}{\phi_1}\big[\phi_6\mathsf{k} + (\phi_7+\phi_8)\delta_b\big]. \quad (59)$$

Eventually, from the constraint (38), we claim that $\mathbb{E}\{\vartheta^T(t)D\vartheta(t)\} < C_2$, which concludes the proof of this theorem. □

3.3. Hybrid control design formulation based on fault alarm technique

In the section that comes next, we expand our control design methodology to encompass two distinct scenarios in which the controller gain matrices are unknown. At first, we construct a control design for a fault-free system. Subsequently, the focus shifts to examining the fault-tolerant technique.

Case (i): Sampled robust control law: When the undertaken system is under the context of free from fault and gain matrices are unknown, the control law is designed as follows:

$$\lambda(t) = \tilde{\mathfrak{H}}_{\mathfrak{j}\nu}^1\beta(t)\big[\alpha(t)\mathfrak{f}(\vartheta(t_{\mathfrak{k}})) + (1-\alpha(t))\vartheta(t_{\mathfrak{k}})\big]. \quad (60)$$

Theorem 3. *Let the Assumptions 1–5 hold and for the pre-stated scalars $\bar{\iota}, \kappa, \mathfrak{y}_1, \mathfrak{y}_2, \bar{\alpha}, \bar{\beta}, \wp$, the closed-loop system (8) is finite-time bounded with respect to $(C_1, C_2, \mathcal{G}_{\mathfrak{w}}, \gamma, D)$ and extended dissipative, if the matrices $\tilde{\mathcal{P}}_{\mathfrak{e}\mathfrak{j}} > 0$, $\tilde{\mathcal{Q}}_{\mathfrak{e}\mathfrak{j}}$ $(\mathfrak{e} = 1,2,3,4)$, $\tilde{\mathcal{S}}_{\mathfrak{j}}$, $\tilde{\mathcal{T}}_{1\mathfrak{j}} > 0$, $\tilde{\mathcal{T}}_{2\mathfrak{j}} > 0$ and $\mathfrak{W}_{\mathfrak{j}\nu}$, $\mathfrak{Y}_{\mathfrak{j}}$ exist, such that the following constraints hold:*

$$\begin{bmatrix} \Lambda_1^{\mathfrak{d}\nu} + \mathfrak{y}_{\mathfrak{k}}\Lambda_2^{\mathfrak{d}\nu} & \sqrt{\mathfrak{y}_{\mathfrak{k}}}\tilde{\mathcal{V}}_a^T & \sqrt{\mathfrak{y}_{\mathfrak{k}}}\mathfrak{y}_2\tilde{\mathcal{V}}_b^T & \mathfrak{Y}_{\mathfrak{j}}\tilde{\mathfrak{C}}_{\mathfrak{j}\mathfrak{d}}^T \\ * & -\tilde{\mathcal{T}}_{2j} & 0 & 0 \\ * & * & -3\tilde{\mathcal{T}}_{2j} & 0 \\ * & * & * & -F_1^{-1} \end{bmatrix} < 0, \quad (61)$$

$$\begin{bmatrix} \Lambda_1^{\mathfrak{d}\nu} + \mathfrak{y}_{\mathfrak{k}}\Lambda_3^{\mathfrak{d}\nu} & \sqrt{\mathfrak{y}_{\mathfrak{k}}}\tilde{\mathcal{W}}_a^T & \sqrt{\mathfrak{y}_{\mathfrak{k}}}\mathfrak{y}_2\tilde{\mathcal{W}}_b^T & \mathfrak{Y}_{\mathfrak{j}}\tilde{\mathfrak{C}}_{\mathfrak{j}\mathfrak{d}}^T \\ * & -\tilde{\mathcal{T}}_{1j} & 0 & 0 \\ * & * & -3\tilde{\mathcal{T}}_{1j} & 0 \\ * & * & * & -F_1^{-1} \end{bmatrix} < 0, \quad (62)$$

$$\tilde{\mathcal{P}}_{\mathfrak{e}\mathfrak{j}} < \mathfrak{i}\tilde{\mathcal{P}}_{\mathfrak{e}\varsigma},\ \tilde{\mathcal{Q}}_{\mathfrak{e}\mathfrak{j}} < \mathfrak{i}\tilde{\mathcal{Q}}_{\mathfrak{e}\varsigma},\ \tilde{\mathcal{S}}_{\mathfrak{j}} < \mathfrak{i}\tilde{\mathcal{S}}_{\varsigma},$$
$$\tilde{\mathcal{T}}_{1\mathfrak{j}} < \mathfrak{i}\tilde{\mathcal{T}}_{1\varsigma},\ \tilde{\mathcal{T}}_{2\mathfrak{j}} < \mathfrak{i}\tilde{\mathcal{T}}_{2\varsigma}, \mathfrak{i} > 1, \forall\, \mathfrak{j}, \varsigma \in \mathcal{M}, \mathfrak{j} \ne \varsigma, \quad (63)$$

$$\frac{1}{\mathsf{a}}\mathcal{P}_{1\mathfrak{j}} - \tilde{\mathfrak{C}}_{\mathfrak{j}\mathfrak{d}}F_4\tilde{\mathfrak{C}}_{\mathfrak{j}\mathfrak{d}} > 0, \quad (64)$$

the average dwell time satisfies

$$\varkappa > \varkappa^* = \frac{\mathcal{G}_{\mathfrak{f}}ln\imath}{ln(\phi_1C_2) - ln\big(\phi_6\mathsf{k} + (\phi_7+\phi_8)\delta_b\big) + \gamma\mathcal{G}_{\mathfrak{w}}}, \quad (65)$$

where

$$\Lambda_1^{\mathfrak{d}\nu} = \Lambda_{11}^{\mathfrak{d}\nu} + \Lambda_{12}^{\mathfrak{d}\nu},\ \Lambda_{11}^{\mathfrak{d}\nu} = \tilde{\Lambda}_{01}^{\mathfrak{d}\nu} + \tilde{\Lambda}_{02}^{\mathfrak{d}\nu} + \tilde{\Lambda}_{03}^{\mathfrak{d}\nu} + \tilde{\Lambda}_{04}^{\mathfrak{d}\nu} + \tilde{\Lambda}_{05}^{\mathfrak{d}\nu} + \tilde{\Lambda}_{06}^{\mathfrak{d}\nu},$$
$\tilde{\Lambda}_{01}^{\mathfrak{d}\nu} = sym\{\Phi_1^T\tilde{\mathcal{P}}_{1\mathfrak{j}}\Phi_8 - \Psi_3^T\tilde{\mathcal{Q}}_{2\mathfrak{j}}\Psi_4 + \gamma\Phi_1^T\tilde{\mathcal{P}}_{1\mathfrak{j}}\Phi_1\}$, $\tilde{\Lambda}_{02}^{\mathfrak{d}\nu} = sym\{\tilde{\mathcal{W}}_a^T\Psi_5 - 2\tilde{\mathcal{W}}_b^T\Phi_6\}$, $\tilde{\Lambda}_{03}^{\mathfrak{d}\nu} = sym\{-\tilde{\mathcal{V}}_a^T\Psi_7 - 2\tilde{\mathcal{V}}_b^T\Phi_7\}$, $\tilde{\Lambda}_{04}^{\mathfrak{d}\nu} = \Psi_1^T\tilde{\mathcal{P}}_{2\mathfrak{j}}\Psi_1 + \Psi_2^T\tilde{\mathcal{P}}_{3\mathfrak{j}}\Psi_2$,
$\tilde{\Lambda}_{05}^{\mathfrak{d}\nu} = \bar{\iota}^2\Phi_1^T\tilde{\mathcal{P}}_{4\mathfrak{j}}\Phi_1 + \Psi_3^T\tilde{\mathcal{Q}}_{1\mathfrak{j}}\Psi_3$, $\tilde{\Lambda}_{06}^{\mathfrak{d}\nu} = \Psi_{10}^T\tilde{\mathcal{Q}}_{3\mathfrak{j}}\Psi_{10} + \Psi_{10}^T\tilde{\mathcal{Q}}_{4\mathfrak{j}}\Psi_4$,

$\Lambda_{12}^{\mathfrak{d}\nu} = sym\{\hat{\Lambda}_{01}^{\mathfrak{d}\nu}\hat{\Lambda}_{02}^{\mathfrak{d}\nu} - \hat{\Lambda}_{03}^{\mathfrak{d}\nu}\} + \hat{\Lambda}_{04}^{\mathfrak{d}\nu} + \hat{\Lambda}_{05}^{\mathfrak{d}\nu} + \hat{\Lambda}_{06}^{\mathfrak{d}\nu}$,

$\hat{\Lambda}_{01}^{\mathfrak{d}\nu} = \Phi_1^T + \Phi_8^T\wp$, $\hat{\Lambda}_{03}^{\mathfrak{d}\nu} = \Phi_1^T\mathfrak{Y}_{\mathfrak{j}}F_2\Phi_{10}$,

$\hat{\Lambda}_{02}^{\mathfrak{d}\nu} = \tilde{\mathfrak{A}}_{\mathfrak{j}\mathfrak{d}}\mathfrak{Y}_{\mathfrak{j}}\Phi_1 + \tilde{\mathfrak{B}}_{\mathfrak{j}\mathfrak{d}}\mathfrak{Y}_{\mathfrak{j}}\Phi_2 + \bar{\beta}\tilde{\mathfrak{B}}_{\mathfrak{j}\mathfrak{d}}\mathfrak{G}\{\bar{\alpha}\mathfrak{W}_{\mathfrak{j}\nu}\Phi_9 + (1-\bar{\alpha})\mathfrak{W}_{\mathfrak{j}\nu}\Phi_4\} + \tilde{\mathfrak{D}}_{\mathfrak{j}\mathfrak{d}}\mathfrak{Y}_{\mathfrak{j}}\Phi_{10} - \mathfrak{Y}_{\mathfrak{j}}\Phi_8$, $\hat{\Lambda}_{04}^{\mathfrak{d}\nu} = -\Phi_{10}^TF_3\Phi_{10} + \Phi_4^T\mathcal{F}^T\tilde{\mathcal{E}}\mathcal{F}\Phi_4 - \Phi_9^T\tilde{\mathcal{E}}\Phi_9$,

$\hat{\Lambda}_{05}^{\mathfrak{d}\nu} = -\Phi_{11}^T(9\tilde{\mathcal{P}}_{4\mathfrak{j}})\Phi_{11} + \Phi_{11}^T\big(\frac{36}{\iota}\tilde{\mathcal{P}}_{4\mathfrak{j}}\big)\Phi_{12} - \Phi_{11}^T\big(\frac{60}{\iota^2}\tilde{\mathcal{P}}_{4\mathfrak{j}}\big)\Phi_{13}$,
$\hat{\Lambda}_{06}^{\mathfrak{d}\nu} = -\Phi_{12}^T\big(\frac{192}{\iota^2}\tilde{\mathcal{P}}_{4\mathfrak{j}}\big)\Phi_{12} + \Phi_{12}^T\big(\frac{360}{\iota^3}\tilde{\mathcal{P}}_{4\mathfrak{j}}\big)\Phi_{13} - \Phi_{13}^T\big(\frac{720}{\iota^4}\tilde{\mathcal{P}}_{4\mathfrak{j}}\big)\Phi_{13}$,

$\Lambda_2^{\mathfrak{d}\nu} = sym\{\Psi_3^T\tilde{\mathcal{Q}}_{1\mathfrak{j}}\Psi_9 + \Psi_9^T\tilde{\mathcal{Q}}_{2\mathfrak{j}}\Psi_4 + \tilde{\mathcal{V}}_b^T\Psi_8\} + \Psi_4^T\tilde{\mathcal{S}}_{\mathfrak{j}}\Psi_4 + \Phi_8^T\tilde{\mathcal{T}}_{1\mathfrak{j}}\Phi_8$,

$\Lambda_3^{\mathfrak{d}\nu} = sym\{\Psi_{10}^T\tilde{\mathcal{Q}}_{3\mathfrak{j}}\Psi_{11} + \Psi_{11}^T\tilde{\mathcal{Q}}_{4\mathfrak{j}}\Psi_4 + \tilde{\mathcal{W}}_b^T\Psi_6\} - \Psi_4^T\tilde{\mathcal{S}}_{\mathfrak{j}}\Psi_4 + \Phi_8^T\tilde{\mathcal{T}}_{2\mathfrak{j}}\Phi_8$.

Further, if the above-given constraints have a feasible solution, then we can determine the gain matrices of the configured control by leveraging the underneath relation:

$$\tilde{\mathfrak{H}}_{\mathfrak{j}\nu}^1 = \mathfrak{W}_{\mathfrak{j}\nu}\mathfrak{Y}_{\mathfrak{j}}^{-1}. \quad (66)$$

Proof. At first, to demonstrate this theorem, we choose the analogous Lyapunov functional (14) which is described in the previous theorem. After that, we replace the control gain $\tilde{\mathfrak{H}}_{\mathfrak{j}\nu}$ with $\tilde{\mathfrak{H}}_{\mathfrak{j}\nu}^1$ and assume $\mathcal{Z}_{1\mathfrak{j}}^{-1} = \mathfrak{Y}_{\mathfrak{j}}$, then pre-and post-multiply by $\mathrm{diag}\{\underbrace{\mathfrak{Y}_{\mathfrak{j}}, \dots, \mathfrak{Y}_{\mathfrak{j}}}_{9\ times}, \underbrace{I, \mathfrak{Y}_{\mathfrak{j}}, \dots, \mathfrak{Y}_{\mathfrak{j}}, I}_{5\ times}\}$. And, with the employment of the Schur complement lemma [36] and by letting $\mathfrak{Y}_{\mathfrak{j}}\mathcal{P}_{\mathfrak{e}\mathfrak{j}}\mathfrak{Y}_{\mathfrak{j}} = \tilde{\mathcal{P}}_{\mathfrak{e}\mathfrak{j}}$, $\mathfrak{Y}_{\mathfrak{j}}\mathcal{Q}_{\mathfrak{e}\mathfrak{j}}\mathfrak{Y}_{\mathfrak{j}} = \tilde{\mathcal{Q}}_{\mathfrak{e}\mathfrak{j}}$, $\mathfrak{Y}_{\mathfrak{j}}\mathcal{S}_{\mathfrak{j}}\mathfrak{Y}_{\mathfrak{j}} = \tilde{\mathcal{S}}_{\mathfrak{j}}$, $\mathfrak{Y}_{\mathfrak{j}}\mathcal{T}_{1\mathfrak{j}}\mathfrak{Y}_{\mathfrak{j}} = \tilde{\mathcal{T}}_{1\mathfrak{j}}$, $\mathfrak{Y}_{\mathfrak{j}}\mathcal{T}_{2\mathfrak{j}}\mathfrak{Y}_{\mathfrak{j}} = \tilde{\mathcal{T}}_{2\mathfrak{j}}$ and $\mathfrak{W}_{\mathfrak{j}\nu} = \sum_{\nu=1}^{\mathfrak{q}}\mathfrak{h}_{\mathfrak{j}\nu}(\mathfrak{E}(t))\mathfrak{W}_{\mathfrak{j}\nu}$, $\tilde{\mathfrak{H}}_{\mathfrak{j}\nu}^1\mathfrak{Y}_{\mathfrak{j}} = \mathfrak{W}_{\mathfrak{j}\nu}$, we end up with the inequalities (61), (62) offered in the theorem statement. Moreover, if the criteria (61)–(65) hold and by following similar manner of the preceding theorem, we can prove that, the closed-loop system (8) is finite-time bounded and extended dissipative. Thus, the proof of this theorem is closed. □

Case (ii): Fault-tolerant control design:

In actuality, faults will arise primarily because of unforeseen changes, factors in the environment, and similar influences. The existence of faults may result in system deterioration or instability. In order to combat this situation, fault-tolerant control will be established to ensure the seamless operation of the implemented system. Subsequently, a mathematical description of fault-tolerant control is laid out as follows:

$$\lambda(t) = \mathfrak{G}\tilde{\mathfrak{H}}_{\mathfrak{j}\nu}^2\beta(t)\big[\alpha(t)\mathfrak{f}(\vartheta(t_{\mathfrak{k}})) + (1-\alpha(t))\vartheta(t_{\mathfrak{k}})\big], \quad (67)$$

where $\mathfrak{G} = diag\{\mathfrak{g}_1, \mathfrak{g}_2, \dots, \mathfrak{g}_n\}$ is the actuator fault matrix. Moreover, the upper and lower bounds of the fault matrix are defined hereunder:

$$0 \le \underline{\mathfrak{G}} = diag\{\underline{\mathfrak{g}}_1, \underline{\mathfrak{g}}_2, \dots, \underline{\mathfrak{g}}_n\} \le \mathfrak{G} = diag\{\mathfrak{g}_1, \mathfrak{g}_2, \dots, \mathfrak{g}_n\} \le \bar{\mathfrak{G}} = diag\{\bar{\mathfrak{g}}_1, \bar{\mathfrak{g}}_2, \dots, \bar{\mathfrak{g}}_n\} \le I,$$

here $\underline{\mathfrak{G}}$ and $\bar{\mathfrak{G}}$ are known and if $\mathfrak{G} = 0$, the investigated system is under complete fault environment, if $\mathfrak{G} = 1$ signifies, then the system is free of fault and if $\mathfrak{G}$ is in between the 0 and 1, the system is under partial actuator failure. Thereafter, the matrix $\mathfrak{G}$ can be constructed as $\mathfrak{G} = \mathfrak{G}_0 + \mathfrak{G}_1\Gamma(t)$, where

$$\mathfrak{G}_0 = diag\{\mathfrak{g}_{01}, \mathfrak{g}_{02}, \dots, \mathfrak{g}_{0n}\} = \frac{\underline{\mathfrak{G}} + \bar{\mathfrak{G}}}{2} = diag\Big\{\frac{\underline{\mathfrak{g}}_1 + \bar{\mathfrak{g}}_1}{2}, \frac{\underline{\mathfrak{g}}_2 + \bar{\mathfrak{g}}_2}{2}, \dots, \frac{\underline{\mathfrak{g}}_n + \bar{\mathfrak{g}}_n}{2}\Big\},$$

$$\mathfrak{G}_1 = diag\{\mathfrak{g}_{11}, \mathfrak{g}_{12}, \dots, \mathfrak{g}_{1n}\} = \frac{\underline{\mathfrak{G}} - \bar{\mathfrak{G}}}{2} = diag\Big\{\frac{\underline{\mathfrak{g}}_1 - \bar{\mathfrak{g}}_1}{2}, \frac{\underline{\mathfrak{g}}_2 - \bar{\mathfrak{g}}_2}{2}, \dots, \frac{\underline{\mathfrak{g}}_n - \bar{\mathfrak{g}}_n}{2}\Big\},$$

and $\Gamma(t)$ aligns with the constraint $\Gamma^T(t)\Gamma(t) \le I$.

Remark 4. We configured the two-sided looped Lyapunov-Krasovskii functional tailored for sampled-data control systems. It uses both parts of each sampling interval, i.e., $t_{\mathfrak{k}}$ to t and t to $t_{\mathfrak{k}+1}$. Unlike a one-sided form that only uses $t_{\mathfrak{k}}$ to t, the two-sided construction links the evolution before and after the sample and requires positive-definiteness only at the sampling instants, so the Lyapunov value may vary between samples. These features reduce conservatism in the LMIs and broaden the certified sampling-period range.

Theorem 4. *For the defined scalars $\bar{\imath}, \kappa, \mathfrak{y}_1, \mathfrak{y}_2, \tilde{\alpha}, \bar{\beta}, \wp$ and the unknown matrix $\mathfrak{G}$, the closed-loop system (8) is finite-time bounded with respect to $(C_1, C_2, \mathcal{G}_{\mathfrak{w}}, \gamma, D)$ and extended dissipative under the Assumptions 1–5, if the positive definite matrices $\tilde{\mathcal{P}}_{\mathfrak{e}\mathfrak{j}}$, $\tilde{\mathcal{T}}_{1\mathfrak{j}}$, $\tilde{\mathcal{T}}_{2\mathfrak{j}}$, matrices $\tilde{\mathcal{Q}}_{\mathfrak{e}\mathfrak{j}}$ $(\mathfrak{e} = 1, 2, 3, 4)$, $\tilde{\mathcal{S}}_{\mathfrak{j}}$, $\mathfrak{W}_{\mathfrak{j}\nu}$ and $\mathfrak{Y}_{\mathfrak{j}}$ exist, such that the ensuing connections hold:*

$$\begin{bmatrix} \tilde{\Lambda}_1^{\mathfrak{d}\nu} + \mathfrak{y}_{\mathfrak{k}}\Lambda_2^{\mathfrak{d}\nu} & \sqrt{\mathfrak{y}_{\mathfrak{k}}}\tilde{\mathcal{V}}_a^T & \sqrt{\mathfrak{y}_{\mathfrak{k}}}\mathfrak{y}_2\tilde{\mathcal{V}}_b^T & \mathfrak{Y}_{\mathfrak{j}}\tilde{\mathfrak{C}}_{\mathfrak{j}\mathfrak{d}}^T & \varphi^{\mathfrak{d}\nu} \\ * & -\tilde{\mathcal{T}}_{2j} & 0 & 0 & 0 \\ * & * & -3\tilde{\mathcal{T}}_{2j} & 0 & 0 \\ * & * & * & -F_1^{-1} & 0 \\ * & * & * & * & \mathfrak{Z}^{\mathfrak{d}\nu} \end{bmatrix} < 0, \tag{68}$$

$$\begin{bmatrix} \tilde{\Lambda}_1^{\mathfrak{d}\nu} + \mathfrak{y}_{\mathfrak{k}}\Lambda_3^{\mathfrak{d}\nu} & \sqrt{\mathfrak{y}_{\mathfrak{k}}}\tilde{\mathcal{W}}_a^T & \sqrt{\mathfrak{y}_{\mathfrak{k}}}\mathfrak{y}_2\tilde{\mathcal{W}}_b^T & \mathfrak{Y}_{\mathfrak{j}}\tilde{\mathfrak{C}}_{\mathfrak{j}\mathfrak{d}}^T & \varphi^{\mathfrak{d}\nu} \\ * & -\tilde{\mathcal{T}}_{1j} & 0 & 0 & 0 \\ * & * & -3\tilde{\mathcal{T}}_{1j} & 0 & 0 \\ * & * & * & -F_1^{-1} & 0 \\ * & * & * & * & \mathfrak{Z}^{\mathfrak{d}\nu} \end{bmatrix} < 0, \tag{69}$$

$$\tilde{\mathcal{P}}_{\mathfrak{e}\mathfrak{j}} < \mathfrak{i}\tilde{\mathcal{P}}_{\mathfrak{e}\varsigma},\ \tilde{\mathcal{Q}}_{\mathfrak{e}\mathfrak{j}} < \mathfrak{i}\tilde{\mathcal{Q}}_{\mathfrak{e}\varsigma},\ \tilde{\mathcal{S}}_{\mathfrak{j}} < \mathfrak{i}\tilde{\mathcal{S}}_{\varsigma},$$
$$\tilde{\mathcal{T}}_{1\mathfrak{j}} < \mathfrak{i}\tilde{\mathcal{T}}_{1\varsigma},\ \tilde{\mathcal{T}}_{2\mathfrak{j}} < \mathfrak{i}\tilde{\mathcal{T}}_{2\varsigma}, \mathfrak{i} > 1, \forall\, \mathfrak{j}, \varsigma \in \mathcal{M}, \mathfrak{j} \neq \varsigma, \tag{70}$$

$$\frac{1}{\mathfrak{a}}\mathcal{P}_{1\mathfrak{j}} - \tilde{\mathfrak{C}}_{\mathfrak{j}\mathfrak{d}}F_4\tilde{\mathfrak{C}}_{\mathfrak{j}\mathfrak{d}} > 0, \tag{71}$$

the average dwell time satisfies

$$\varkappa > \varkappa^* = \frac{\mathcal{G}_{\mathfrak{f}} ln\imath}{ln(\phi_1 C_2) - ln\big(\phi_6 \mathsf{k} + (\phi_7 + \phi_8)\delta_b\big) + \gamma\mathcal{G}_{\mathfrak{w}}}, \tag{72}$$

where

$$\tilde{\Lambda}_1^{\mathfrak{d}\nu} = \Lambda_{11}^{\mathfrak{d}\nu} + \check{\Lambda}_{12}^{\mathfrak{d}\nu},$$
$$\check{\Lambda}_{12}^{\mathfrak{d}\nu} = sym\big\{\hat{\Lambda}_{01}^{\mathfrak{d}\nu}\check{\Lambda}_{02}^{\mathfrak{d}\nu} - \hat{\Lambda}_{03}^{\mathfrak{d}\nu}\big\} + \hat{\Lambda}_{04}^{\mathfrak{d}\nu} + \hat{\Lambda}_{05}^{\mathfrak{d}\nu} + \hat{\Lambda}_{06}^{\mathfrak{d}\nu},$$
$$\check{\Lambda}_{02}^{\mathfrak{d}\nu} = \tilde{\mathfrak{A}}_{\mathfrak{j}\mathfrak{d}}\mathfrak{Y}_{\mathfrak{j}}\Phi_1 + \tilde{\mathfrak{V}}_{\mathfrak{j}\mathfrak{d}}\mathfrak{Y}_{\mathfrak{j}}\Phi_2 + \bar{\beta}\tilde{\mathfrak{B}}_{\mathfrak{j}\mathfrak{d}}\mathfrak{G}_0\{\tilde{\alpha}\mathfrak{W}_{\mathfrak{j}\nu}\Phi_9 + (1-\tilde{\alpha})\mathfrak{W}_{\mathfrak{j}\nu}\Phi_4\} + \tilde{\mathfrak{D}}_{\mathfrak{j}\mathfrak{d}}\mathfrak{Y}_{\mathfrak{j}}\Phi_{10} - \mathfrak{Y}_{\mathfrak{j}}\Phi_8,\ \varphi_{(1,1)}^{\mathfrak{d}\nu} = \bar{\beta}(1-\tilde{\alpha})\omega_1\tilde{\mathfrak{B}}_{\mathfrak{j}\mathfrak{d}}\mathfrak{G}_1,\ \varphi_{(1,3)}^{\mathfrak{d}\nu} = \bar{\beta}\tilde{\alpha}\omega_2\tilde{\mathfrak{B}}_{\mathfrak{j}\mathfrak{d}}\mathfrak{G}_1,$$
$$\varphi_{(4,2)}^{\mathfrak{d}\nu} = \mathfrak{W}_{\mathfrak{j}\nu}^T,\ \varphi_{(4,5)}^{\mathfrak{d}\nu} = (\wp\bar{\beta}\tilde{\alpha}\omega_3\tilde{\mathfrak{B}}_{\mathfrak{j}\mathfrak{d}}\mathfrak{G}_1)^T,\ \varphi_{(9,4)}^{\mathfrak{d}\nu} = \mathfrak{W}_{\mathfrak{j}\nu}^T,\ \varphi_{(8,6)}^{\mathfrak{d}\nu} = \mathfrak{W}_{\mathfrak{j}\nu}^T,\ \varphi_{(8,7)}^{\mathfrak{d}\nu} = (\wp\bar{\beta}(1-\tilde{\alpha})\omega_4\tilde{\mathfrak{B}}_{\mathfrak{j}\mathfrak{d}}\mathfrak{G}_1),\ \varphi_{(9,8)}^{\mathfrak{d}\nu} = \mathfrak{W}_{\mathfrak{j}\nu}^T,\ \mathfrak{Z}^{\mathfrak{d}\nu} = diag\{-\omega_1\mathbb{I}, -\omega_1\mathbb{I}, -\omega_2\mathbb{I}, -\omega_2\mathbb{I}, -\omega_3\mathbb{I}, -\omega_3\mathbb{I}, -\omega_4\mathbb{I}, -\omega_4\mathbb{I}\}.$$

Moreover, if the above-listed constraints have a feasible environment, we can determine the gain matrices by utilizing the below constraint

$$\tilde{\mathfrak{H}}_{\mathfrak{j}\nu}^2 = \mathfrak{W}_{\mathfrak{j}\nu}\mathfrak{Y}_{\mathfrak{j}}^{-1}. \tag{73}$$

Proof. The mathematical argument of this theorem is based on the same strategy that was worked upon in the proofs of earlier theorems. Initially substitute $\tilde{\mathfrak{H}}_{\mathfrak{j}\nu}^1$ as $[\mathfrak{G}_0 + \mathfrak{G}_1\Gamma(t)]\tilde{\mathfrak{H}}_{\mathfrak{j}\nu}^2$ in the conditions (61), (62). After that, we can demonstrate our inequalities (68), (69) which is laid out in the statement of the theorem using the Schur complement lemma [36] and the S-Procedure along with some straightforward mathematical calculations. Ultimately, guided by Lyapunov stability theory and Definitions 1 and 2, we can substantiate the fundamental objective of this section for the closed-loop architecture under fault-tolerant control, thereby completing the evidence of this theorem. □

3.4. Observer model design

The present portion sets forth the hybrid control law, blending robust and fault-tolerant control within the framework of fault alarm strategies. Precisely, the fault alarm technique is employed to assign control whenever the system detects failures in the actuator module. When the system is experiencing a fault, the fault-tolerant control mechanism will start operating, while the robust control law will take over once the system is no longer experiencing a failure. On top of that, since fault alarm relies on cutoff values, it's important to choose threshold values that will eventually ignore false switching at redundant times. Accordingly, the following form governs a residual observer to accurately activate the fault-tolerant controller:

$$\begin{aligned} \dot{\hat{\vartheta}}(t) &= \tilde{\mathfrak{A}}_{\mathfrak{j}\mathfrak{d}}\hat{\vartheta}(t) + \tilde{\mathfrak{V}}_{\mathfrak{j}\mathfrak{d}}\hat{\vartheta}(t-\imath(t)) + \tilde{\mathfrak{B}}_{\mathfrak{j}\mathfrak{d}}\lambda^f(t) + \tilde{\mathcal{B}}_{\mathfrak{j}\mathfrak{d}}(\xi(t) - \hat{\xi}(t)), \\ \hat{\xi}(t) &= \tilde{\mathfrak{C}}_{\mathfrak{j}\mathfrak{d}}\hat{\vartheta}(t), \end{aligned} \tag{74}$$

where $\hat{\vartheta}(t)$ and $\hat{\xi}(t)$ epitomize the state and output vector of the observer layout, respectively; $\lambda^f(t)$ indicates the control input to the actuator component; $\tilde{\mathcal{B}}_{\mathfrak{j}\mathfrak{d}} = \sum_{\mathfrak{d}=1}^{\mathfrak{q}} \mathfrak{h}_{\mathfrak{j}\mathfrak{d}}(\mathfrak{E}(t))\mathcal{B}_{\mathfrak{j}\mathfrak{d}}$ represents the gain matrices of the established observer and its determining process is similar to previous theorem portions.

3.5. Fault-alarm driven hybrid control law configuration

Subsequently, let us define the error vector $\tilde{\vartheta}(t) = \vartheta(t) - \hat{\vartheta}(t)$ and then by using (4) and (74), we can directly attain the following relation:

$$\dot{\tilde{\vartheta}}(t) = \tilde{\mathfrak{A}}_{\mathfrak{j}\mathfrak{d}}\tilde{\vartheta}(t) + \tilde{\mathfrak{V}}_{\mathfrak{j}\mathfrak{d}}\tilde{\vartheta}(t-\imath(t)) + \tilde{\mathfrak{B}}_{\mathfrak{j}\mathfrak{d}}(\lambda(t) - \lambda^f(t)) - \tilde{\mathcal{B}}_{\mathfrak{j}\mathfrak{d}}\tilde{\mathfrak{C}}_{\mathfrak{j}\mathfrak{d}}\tilde{\vartheta}(t) + \tilde{\mathfrak{D}}_{\mathfrak{j}\mathfrak{d}}\delta(t). \tag{75}$$

Given an overall standard, an actuator component of the specified model will usually be impacted by both faulty as well as fault-free circumstances. From this vantage point, the hybrid controller can handle both kinds of scenarios. Specifically, the above equation has been modified to take the form indicated below when there is no actuator failure, that is, when $\lambda(t) = \lambda^f(t)$ in the error system (75).

$$\dot{\tilde{\vartheta}}(t) = \tilde{\mathfrak{A}}_{\mathfrak{j}\mathfrak{d}}\tilde{\vartheta}(t) + \tilde{\mathfrak{V}}_{\mathfrak{j}\mathfrak{d}}\tilde{\vartheta}(t-\imath(t)) - \tilde{\mathcal{B}}_{\mathfrak{j}\mathfrak{d}}\tilde{\mathfrak{C}}_{\mathfrak{j}\mathfrak{d}}\tilde{\vartheta}(t) + \tilde{\mathfrak{D}}_{\mathfrak{j}\mathfrak{d}}\delta(t). \tag{76}$$

On the contrary, whenever the error model (75) encounters faulty circumstance, that is $\lambda(t) = \mathfrak{G}\lambda^f(t)$, we end-up with the below given equation:

$$\dot{\tilde{\vartheta}}(t) = \tilde{\mathfrak{A}}_{\mathfrak{j}\mathfrak{d}}\tilde{\vartheta}(t) + \tilde{\mathfrak{V}}_{\mathfrak{j}\mathfrak{d}}\tilde{\vartheta}(t-\imath(t)) + \tilde{\mathfrak{B}}_{\mathfrak{j}\mathfrak{d}}(\mathfrak{G} - I)\lambda^f(t) - \tilde{\mathcal{B}}_{\mathfrak{j}\nu}\tilde{\mathfrak{C}}_{\mathfrak{j}\mathfrak{d}}\tilde{\vartheta}(t) + \tilde{\mathfrak{D}}_{\mathfrak{j}\mathfrak{d}}\delta(t). \tag{77}$$

Additionally, the system will become unstable and fail to converge to the equilibrium point if an actuator fails. Therefore, it is critical in establishing a threshold value in order to identify the fault. Hence, we can make a significant inference about the relationship between error residue and external disturbance from Eq. (76):

$$\big[\tilde{\mathcal{B}}_{\mathfrak{j}\nu}\tilde{\mathfrak{C}}_{\mathfrak{j}\mathfrak{d}} - \tilde{\mathfrak{A}}_{\mathfrak{j}\mathfrak{d}} - \tilde{\mathfrak{B}}_{\mathfrak{j}\mathfrak{d}}\big]\tilde{\vartheta}(t) = \tilde{\mathfrak{D}}_{\mathfrak{j}\mathfrak{d}}\delta_b, \tag{78}$$

wherein δ_b points the upper bound of the disturbance $\delta(t)$. From there, we straightforwardly obtain the underneath equation:

$$\| \mathsf{Z}(t) \| \leq \| \chi_{\mathfrak{j}\mathfrak{d}}\delta_b \| \leq \| \chi_{\mathfrak{j}\mathfrak{d}} \| \| \delta_b \|, \tag{79}$$

where $\chi_{\mathfrak{j}\mathfrak{d}} = \| \tilde{\mathfrak{C}}_{\mathfrak{j}\mathfrak{d}}(\tilde{\mathcal{B}}_{\mathfrak{j}\mathfrak{d}}\tilde{\mathfrak{C}}_{\mathfrak{j}\mathfrak{d}} - \tilde{\mathfrak{A}}_{\mathfrak{j}\mathfrak{d}} - \tilde{\mathfrak{B}}_{\mathfrak{j}\mathfrak{d}})^+\tilde{\mathfrak{D}}_{\mathfrak{j}\mathfrak{d}} \|$ and $\mathsf{Z}(t) = \xi(t) - \hat{\xi}(t)$. Further, we design the threshold as $\mathcal{O} = \| \chi_{\mathfrak{j}\mathfrak{d}} \| \| \delta_b \|$. In this instance, we deploy the algorithm [13] in order to pinpoint the location of the fault and to send an alarm to the controller in the following manner:

$$\mathsf{N}(t) = \begin{cases} 0, & \text{do not switch if } \|\mathsf{Z}(t)\| \leq \mathcal{O}, \\ 1, & \text{switch if } \|\mathsf{Z}(t)\| > \mathcal{O}. \end{cases}$$

Ultimately, utilizing the aforementioned technique, the hybrid control in the context of fault alarm is formulated as follows:

$$\lambda^{f}(t) = \big(1-\mathsf{N}(t)\big)\big[\tilde{\mathfrak{H}}^{1}_{\mathrm{j}\nu}\beta(t)\big(\alpha(t)\mathfrak{f}(\vartheta(t_{\mathfrak{k}}))+(1-\alpha(t))\vartheta(t_{\mathfrak{k}})\big)\big] + \mathsf{N}(t)\big[\tilde{\mathfrak{H}}^{2}_{\mathrm{j}\nu}\beta(t)\big(\alpha(t)\mathfrak{f}(\vartheta(t_{\mathfrak{k}}))+(1-\alpha(t))\vartheta(t_{\mathfrak{k}})\big)\big].$$

3.6. Stability requirements for the NSFSs in the absence of time delay

To exemplify the use of the suggested stability requirements, we develop a corollary for the specific situation devoid of time delay. In this connection, by considering the absence of time-varying delay in the system under examination (4), we obtain the subsequent closed-loop system:

$$\begin{aligned}\dot{\vartheta}(t) =& \tilde{\mathfrak{A}}_{\mathrm{j}\mathfrak{d}}\vartheta(t)+\tilde{\mathfrak{B}}_{\mathrm{j}\mathfrak{d}}\mathfrak{G}\lambda(t)+\tilde{\mathfrak{D}}_{\mathrm{j}\mathfrak{d}}\delta(t),\\ \xi(t) =& \tilde{\mathfrak{C}}_{\mathrm{j}\mathfrak{d}}\vartheta(t).\end{aligned} \tag{80}$$

Corollary 1. *Under the Assumptions 1–5, for the known constants $\mathfrak{y}_1,\mathfrak{y}_2,\bar{\alpha},\bar{\beta},\wp$ and the unknown matrix $\mathfrak{G}$, the closed-loop system (80) is finite-time bounded with respect to $(C_1,C_2,\mathcal{G}_{\mathfrak{w}},\gamma,\mathcal{D})$ and extended dissipative, if there exist positive definite matrices $\tilde{\mathcal{P}}_{1\mathrm{j}}$, $\tilde{\mathcal{T}}_{1\mathrm{j}}$, $\tilde{\mathcal{T}}_{2\mathrm{j}}$, matrices $\tilde{\mathcal{Q}}_{\mathfrak{e}\mathrm{j}}$ ($\mathfrak{e}=1,2,3,4$), $\tilde{\mathcal{S}}_{\mathrm{j}}$, $\mathfrak{W}_{\mathrm{j}\nu}$ and $\mathfrak{Y}_{\mathrm{j}}$, such that the below-give conditions hold:*

$$\begin{bmatrix}\Upsilon_1^{\mathfrak{d}\nu}+\mathfrak{y}_{\mathfrak{k}}\Upsilon_2^{\mathfrak{d}\nu} & \sqrt{\mathfrak{y}_{\mathfrak{k}}}\tilde{\mathcal{V}}_a^T & \sqrt{\mathfrak{y}_{\mathfrak{k}}}\mathfrak{y}_2\tilde{\mathcal{V}}_b^T & \mathfrak{Y}_{\mathrm{j}}\tilde{\mathfrak{C}}_{\mathrm{j}\mathfrak{d}}^T & \varphi^{\mathfrak{d}\nu}\\ * & -\tilde{\mathcal{T}}_{2j} & 0 & 0 & 0\\ * & * & -3\tilde{\mathcal{T}}_{2j} & 0 & 0\\ * & * & * & -F_1^{-1} & 0\\ * & * & * & * & \mathfrak{Z}^{\mathfrak{d}\nu}\end{bmatrix} < 0, \tag{81}$$

$$\begin{bmatrix}\Upsilon_1^{\mathfrak{d}\nu}+\mathfrak{y}_{\mathfrak{k}}\Upsilon_3^{\mathfrak{d}\nu} & \sqrt{\mathfrak{y}_{\mathfrak{k}}}\tilde{\mathcal{W}}_a^T & \sqrt{\mathfrak{y}_{\mathfrak{k}}}\mathfrak{y}_2\tilde{\mathcal{W}}_b^T & \mathfrak{Y}_{\mathrm{j}}\tilde{\mathfrak{C}}_{\mathrm{j}\mathfrak{d}}^T & \varphi^{\mathfrak{d}\nu}\\ * & -\tilde{\mathcal{T}}_{1j} & 0 & 0 & 0\\ * & * & -3\tilde{\mathcal{T}}_{1j} & 0 & 0\\ * & * & * & -F_1^{-1} & 0\\ * & * & * & * & \mathfrak{Z}^{\mathfrak{d}\nu}\end{bmatrix} < 0, \tag{82}$$

$$\frac{1}{\mathsf{a}}\mathcal{P}_{1\mathrm{j}}-\tilde{\mathfrak{C}}_{\mathrm{j}\mathfrak{d}F_4}\tilde{\mathfrak{C}}_{\mathrm{j}\mathfrak{d}}>0, \tag{83}$$

$$\begin{aligned}&\tilde{\mathcal{P}}_{1\mathrm{j}}<\mathrm{i}\tilde{\mathcal{P}}_{1\varsigma},\ \tilde{\mathcal{Q}}_{\mathfrak{e}\mathrm{j}}<\mathrm{i}\tilde{\mathcal{Q}}_{\mathfrak{e}\varsigma},\ \tilde{\mathcal{S}}_{\mathrm{j}}<\mathrm{i}\tilde{\mathcal{S}}_{\varsigma},\\ &\tilde{\mathcal{T}}_{1\mathrm{j}}<\mathrm{i}\tilde{\mathcal{T}}_{1\varsigma},\ \tilde{\mathcal{T}}_{2\mathrm{j}}<\mathrm{i}\tilde{\mathcal{T}}_{2\varsigma},\mathrm{i}>1,\forall\,\mathrm{j},\varsigma\in\mathcal{M},\mathrm{j}\neq\varsigma,\end{aligned} \tag{84}$$

the average dwell time satisfies

$$\varkappa>\varkappa^{*}=\frac{\mathcal{G}_{\mathfrak{f}}ln\imath}{ln(\phi_1C_2)-ln\big(\phi_6\mathsf{k}+(\phi_7+\phi_8)\delta_b\big)+\gamma\mathcal{G}_{\mathfrak{w}}}, \tag{85}$$

where

$\Upsilon_1^{\mathfrak{d}\nu}=\Upsilon_{11}^{\mathfrak{d}\nu}+\Upsilon_{12}^{\mathfrak{d}\nu}$, $\Upsilon_{11}^{\mathfrak{d}\nu}=\tilde{\Upsilon}_{01}^{\mathfrak{d}\nu}+\tilde{\Upsilon}_{02}^{\mathfrak{d}\nu}+\tilde{\Upsilon}_{03}^{\mathfrak{d}\nu}+\tilde{\Upsilon}_{04}^{\mathfrak{d}\nu}+\tilde{\Upsilon}_{05}^{\mathfrak{d}\nu}$, $\tilde{\Upsilon}_{01}^{\mathfrak{d}\nu}=sym\big\{\Phi_1^T\tilde{\mathcal{P}}_{1\mathrm{j}}\Phi_8-\Psi_1^T\tilde{\mathcal{Q}}_{2\mathrm{j}}\Psi_2+\gamma\Phi_1^T\tilde{\mathcal{P}}_{1\mathrm{j}}\Phi_1\big\}$, $\tilde{\Upsilon}_{02}^{\mathfrak{d}\nu}=sym\big\{\tilde{\mathcal{W}}_a^T\Psi_3-2\tilde{\mathcal{W}}_b^T\Phi_6\big\}$, $\tilde{\Upsilon}_{03}^{\mathfrak{d}\nu}=sym\big\{-\tilde{\mathcal{V}}_a^T\Psi_5-2\tilde{\mathcal{V}}_b^T\Phi_7\big\}$, $\tilde{\Upsilon}_{04}^{\mathfrak{d}\nu}=\Psi_1^T\tilde{\mathcal{Q}}_{1\mathrm{j}}\Psi_1$, $\tilde{\Upsilon}_{05}^{\mathfrak{d}\nu}=\Psi_8^T\tilde{\mathcal{Q}}_{3\mathrm{j}}\Psi_8+\Psi_8^T\tilde{\mathcal{Q}}_{4\mathrm{j}}\Psi_2$, $\check{\Upsilon}_{12}^{\mathfrak{d}\nu}=sym\big\{\hat{\Upsilon}_{01}^{\mathfrak{d}\nu}\check{\Upsilon}_{02}^{\mathfrak{d}\nu}-\hat{\Upsilon}_{03}^{\mathfrak{d}\nu}\big\}+\hat{\Upsilon}_{04}^{\mathfrak{d}\nu}$,

$\hat{\Upsilon}_{01}^{\mathfrak{d}\nu}=\Phi_1^T+\Phi_8^T\wp$, $\hat{\Upsilon}_{03}^{\mathfrak{d}\nu}=\Phi_1^T\mathfrak{Y}_{\mathrm{j}F2}\Phi_{10}$,

$\check{\Upsilon}_{02}^{\mathfrak{d}\nu}=\tilde{\mathfrak{A}}_{\mathrm{j}\mathfrak{d}}\mathfrak{Y}_{\mathrm{j}}\Phi_1+\tilde{\mathfrak{V}}_{\mathrm{j}\mathfrak{d}}\mathfrak{Y}_{\mathrm{j}}\Phi_2+\bar{\beta}\tilde{\mathfrak{B}}_{\mathrm{j}\mathfrak{d}}\mathfrak{G}_0\{\bar{\alpha}\tilde{\mathfrak{W}}_{\mathrm{j}\nu}\Phi_9+(1-\bar{\alpha})\tilde{\mathfrak{W}}_{\mathrm{j}\nu}\Phi_4\}+\tilde{\mathfrak{D}}_{\mathrm{j}\mathfrak{d}}\mathfrak{Y}_{\mathrm{j}}\Phi_{10}-\mathfrak{Y}_{\mathrm{j}}\Phi_8$, $\hat{\Upsilon}_{04}^{\mathfrak{d}\nu}=-\Phi_{10}^TF_3\Phi_{10}+\Phi_4^T\mathcal{F}^T\tilde{\mathcal{E}}\mathcal{F}\Phi_4-\Phi_9^T\tilde{\mathcal{E}}\Phi_9$,

$\Upsilon_2^{\mathfrak{d}\nu}=sym\big\{\Psi_1^T\tilde{\mathcal{Q}}_{1\mathrm{j}}\Psi_7+\Psi_7^T\tilde{\mathcal{Q}}_{2\mathrm{j}}\Psi_2+\check{\mathcal{V}}_b^T\Psi_6\big\}+\Psi_2^T\tilde{\mathcal{S}}_{\mathrm{j}}\Psi_2+\Phi_8^T\tilde{\mathcal{T}}_{1\mathrm{j}}\Phi_8$,

$\Upsilon_3^{\mathfrak{d}\nu}=sym\big\{\Psi_8^T\tilde{\mathcal{Q}}_{3\mathrm{j}}\Psi_9+\Psi_9^T\tilde{\mathcal{Q}}_{4\mathrm{j}}\Psi_2+\check{\mathcal{W}}_b^T\Psi_4\big\}-\Psi_2^T\tilde{\mathcal{S}}_{\mathrm{j}}\Psi_2+\Phi_8^T\tilde{\mathcal{T}}_{2\mathrm{j}}\Phi_8$,

$\varphi_{(1,1)}^{\mathfrak{d}\nu}=\bar{\beta}(1-\bar{\alpha})\omega_1\tilde{\mathfrak{B}}_{\mathrm{j}\mathfrak{d}}\mathfrak{G}_1$, $\varphi_{(1,3)}^{\mathfrak{d}\nu}=\bar{\beta}\bar{\alpha}\omega_2\tilde{\mathfrak{B}}_{\mathrm{j}\mathfrak{d}}\mathfrak{G}_1$, $\varphi_{(4,2)}^{\mathfrak{d}\nu}=\tilde{\mathfrak{W}}_{\mathrm{j}\nu}^T$, $\varphi_{(4,5)}^{\mathfrak{d}\nu}=(\wp\bar{\beta}\bar{\alpha}\omega_3\tilde{\mathfrak{B}}_{\mathrm{j}\mathfrak{d}}\mathfrak{G}_1)^T$, $\varphi_{(9,4)}^{\mathfrak{d}\nu}=\tilde{\mathfrak{W}}_{\mathrm{j}\nu}^T$, $\varphi_{(8,6)}^{\mathfrak{d}\nu}=\tilde{\mathfrak{W}}_{\mathrm{j}\nu}^T$, $\varphi_{(8,7)}^{\mathfrak{d}\nu}=(\wp\bar{\beta}(1-\bar{\alpha})\omega_4\tilde{\mathfrak{B}}_{\mathrm{j}\mathfrak{d}}\mathfrak{G}_1)$, $\varphi_{(9,8)}^{\mathfrak{d}\nu}=\tilde{\mathfrak{W}}_{\mathrm{j}\nu}^T$,

$\Psi_1=col\{\Phi_1-\Phi_4,\ \Phi_6\}$, $\Psi_2=col\{\Phi_4,\ \Phi_5\}$, $\Psi_3=\Phi_1-\Phi_4$, $\Psi_4=\Phi_1+\Phi_4$, $\Psi_5=\Phi_1-\Phi_5$, $\Psi_6=\Phi_1+\Phi_5$, $\Psi_7=col\{\Phi_8,\ \Phi_1\}$, $\Psi_8=col\{\Phi_1-\Phi_5,\ \Phi_7\}$, $\Psi_9=col\{\Phi_8,\ -\Phi_1\}$.

Table 1
Gain matrices of the sampled robust and fault-tolerant control.

Mode	j = 1, ν = 1	j = 1, ν = 2	j = 2, ν = 1	j = 2, ν = 2
$\mathfrak{H}^1_{\mathrm{j}\nu}$	$\begin{bmatrix}-176.89\\-30.81\end{bmatrix}^T$	$\begin{bmatrix}-176.89\\-30.81\end{bmatrix}^T$	$\begin{bmatrix}-66.71\\27.80\end{bmatrix}^T$	$\begin{bmatrix}-66.71\\27.80\end{bmatrix}^T$
$\mathfrak{H}^2_{\mathrm{j}\nu}$	$10^4\times\begin{bmatrix}-3.24\\-0.73\end{bmatrix}^T$	$10^4\times\begin{bmatrix}-3.25\\-0.73\end{bmatrix}^T$	$10^3\times\begin{bmatrix}-9.87\\3.49\end{bmatrix}^T$	$10^3\times\begin{bmatrix}-9.87\\3.49\end{bmatrix}^T$

Proof. The demonstration of this corollary follows that of the preceding theorems; therefore, it is omitted here. □

Remark 5. Compared with existing hybrid controllers, our scheme has three distinguishing elements. First, a two-sided looped Lyapunov functional couples the pre- and post-sample evolution over $t_{\mathfrak{k}}$ to t and t to $t_{\mathfrak{k}+1}$, which reduces conservatism. Second, a residual-based fault alarm swiftly triggers switching to the fault-tolerant controller only when needed, yielding a fast reaction at fault onset without running the fault-tolerant mode continuously. Third, we explicitly model hybrid cyberattacks on the control channel and synthesize the law to preserve stability under such non-idealities. Together, these ingredients deliver certified finite-time performance with longer sampling periods and enhanced resilience, clearly differentiating the proposed mechanism from prior hybrid control designs.

4. Numerical simulation

This segment presents two examples to showcase the practical application and benefits of the proposed control law. In particular, the finite-time boundedness of the examined model under the two switching rules and two fuzzy rules has been assessed in the initial example. Consequently, the single-link robot arm model is examined to ascertain the importance and relevance of the acquired findings.

Example 1. Let us consider the system (4) with two rules under the context of multiple vulnerable factors. The matrix associated with the system are given below:

Subsystem 1:

$$\mathfrak{A}_{11}=\begin{bmatrix}2&10\\-1&-1\end{bmatrix},\ \mathfrak{A}_{12}=\begin{bmatrix}2.9&10\\-1&-1\end{bmatrix},\ \mathfrak{V}_{11}=\begin{bmatrix}0.2&0.4\\-0.1&-0.1\end{bmatrix},$$

$$\mathfrak{V}_{12}=\begin{bmatrix}0.4&1.2\\0.7&0.7\end{bmatrix},\ \mathfrak{B}_{11}=\mathfrak{B}_{12}=[0\ 1]^T,$$

$\mathfrak{D}_{11}=[0\ 0.9]^T$, $\mathfrak{D}_{12}=[0\ 0.98]^T$, $\mathfrak{C}_{11}=[1\ 0.1]^T$ and $\mathfrak{C}_{12}=[0.9\ 0.8]^T$.

Subsystem 2:

$$\mathfrak{A}_{21}=\begin{bmatrix}2&10\\-1&-2\end{bmatrix},\ \mathfrak{A}_{22}=\begin{bmatrix}2.9&10\\-1&-2\end{bmatrix},\ \mathfrak{V}_{21}=\begin{bmatrix}1.2&1.4\\-1.1&-1.1\end{bmatrix},$$

$$\mathfrak{V}_{22}=\begin{bmatrix}1.4&1.5\\1.7&1.7\end{bmatrix},\ \mathfrak{B}_{21}=\mathfrak{B}_{22}=[0\ 1]^T,$$

$\mathfrak{D}_{21}=[0\ 0.85]^T$, $\mathfrak{D}_{22}=[0\ 0.8]^T$, $\mathfrak{C}_{21}=[0.5\ 0.7]^T$ and $\mathfrak{C}_{22}=[0.6\ 0.5]^T$.

Furthermore, the bounds of time-varying delay are taken as $\bar{\imath}=0.8$ and $\kappa=0.3$. The interval for the fault is chosen as $\mathfrak{G}\in[0.1,0.3]$. The scalars in the finite-time notion are picked as $C_1=1$, $C_2=4$, $\mathcal{G}_{\mathfrak{w}}=4$, $\delta_b=0.5$. The parameters involved in sampled-data control are $\mathfrak{y}_1=0.001$, $\mathfrak{y}_2=0.2$. The remaining parameters which are part of the feasibility assignment are taken as $\bar{\alpha}=0.1$, $\bar{\beta}=0.8$, $\mathcal{F}=diag\{0.5,0.5\}$, $F_1=-0.8$, $F_2=0.9$, $F_3=0.7$ and $\gamma=1.5$. By deploying these parameters in the MATLAB environment and solving the adequate criteria (68)–(72) that are established in Theorem 4, we procure the gain matrices of the designed hybrid controller which are given in Table 1.

Upon wrapping up the feasibility task, the next initiation of the simulation activity requires the following functions and conditions. The

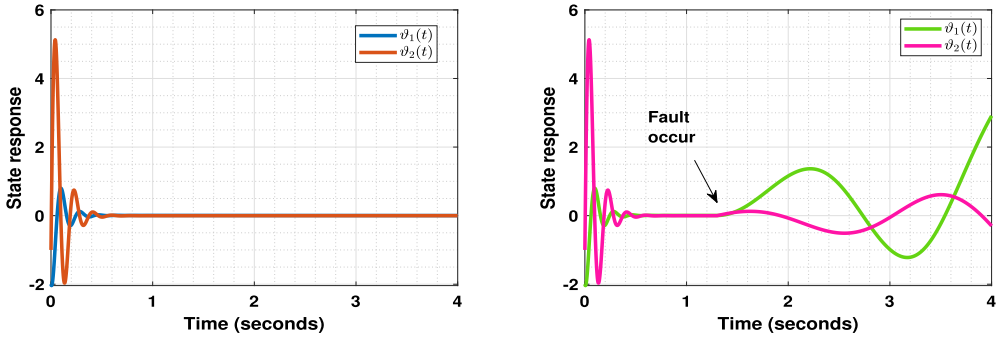

(a) Fault-free environment (b) Fault environment

Fig. 2. State response of the system under robust control.

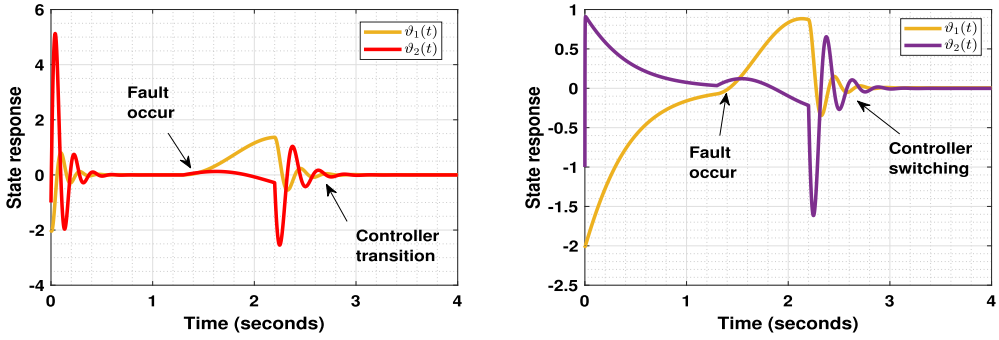

(a) Case (iii) (b) Case (iv)

Fig. 3. State response of the investigated model based on the hybrid control.

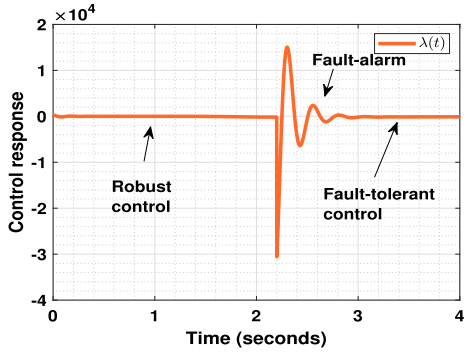

Fig. 4. Hybrid control response.

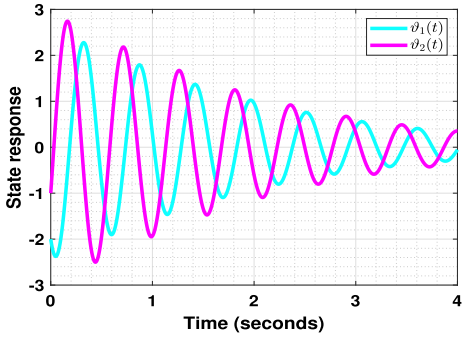

Fig. 5. State response of the model without control.

disturbance and time-delay function are chosen as $\delta(t) = 0.5\sin(t)$ and $\iota(t) = 0.5+0.3\cos(t)$, respectively. The deception attack function is picked up as $\mathfrak{f}(\vartheta(t)) = 0.5\sin(\vartheta(t))$. The initial condition for the examined system is chosen as $\vartheta(t_0) = [-2 \ \ -1]^T$. The membership function are selected as

$$\mathfrak{E}^1_\rho(\vartheta_1(t)) = \begin{cases} \frac{1-(\vartheta_1(t))^2}{9}, & -3 \le \vartheta_1(t) \le 3 \\ 0, & \text{otherwise} \end{cases},$$

$$\mathfrak{E}^2_\rho(\vartheta_1(t)) = 1 - \mathfrak{E}^1_\rho(\vartheta_1(t)), \quad \rho = 1, 2.$$

Following that, through utilizing the previously mentioned matrices, scalars, and conditions, the simulation duty is conducted under the sampling time 0.01, and the resulting graphics are displayed in Figs. 2–7. In particular, the state trajectories of the examined model under the sampled robust control law in the absence of faults are illustrated in Fig. 2(a). In turn, from Fig. 2(b), it is viable that, when the system experiences failures within the framework of sampled robust control, the system states diverge, indicating that the established control law is lacking in managing the effects of faults. Moreover, the state responses of the implemented model via the sampled hybrid control are displayed in Fig. 3 under two cases. Specifically, Case (iii) State response of the system under the designed secured hybrid control law, Case (iv) State response of the system under traditional hybrid control law [14]. From, Fig. 3 it is evident that, following the occurrence of a fault in the control law, the controller transitions to a fault-tolerant mode utilizing a fault alarm indication mechanism. The states' performance is seamless when transitioned to the fault-tolerant mode, emphasizing the importance of the established hybrid control law. Besides, in Case (iii), the state trajectories converge smoothly toward the equilibrium point within a short

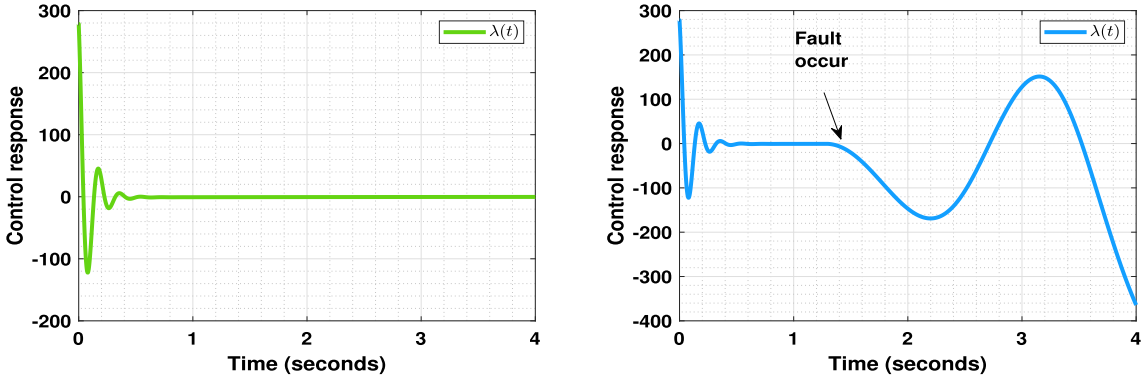

(a) Fault-free case (b) Fault case

Fig. 6. Control trajectories in the context of robust control.

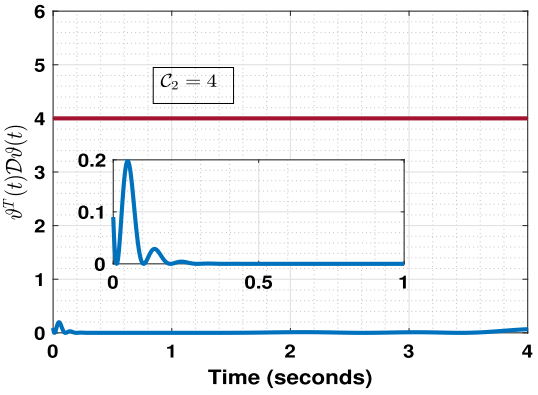

Fig. 7. Time profile of state trajectory.

period whereas, in Case (iv), state responses experience larger fluctuations and take longer to settle. The convergence is noticeably slower, and the transient oscillations persist for a longer duration compared with Case (iii). This brings out the imperative of setting up the secure hybrid control rule. Further, the hybrid control law response is presented in Fig. 4. And, by excluding the control law from the model's overall framework, the paths of the states are shown in Fig. 5, where the divergence of the states underscores the necessity of constructing the control law for the presented model. Moreover, the control responses when the system is free of fault and is subject to fault are showcased in Fig. 6. Added to that, the response of $\vartheta^T(t)\mathcal{D}\vartheta(t)$ is plotted in Fig. 7, in which states are under the prescribed bound that confirms the finite-time boundedness of the investigated system. In summary, the simulated facts point out that over actuator failure, the modeled controller starts functioning rapidly in accordance with the fault alarm system's signal. Further, evaluation discloses that the fault alarm-based hybrid controller can successfully manage unexpected actuator defects in the system and also assist the system in achieving stability despite cyberattacks, external disruptions, actuator malfunctions, and time delays.

The practical relevance of the established result in Corollary 1 is shown by in the following example. In order to achieve this, we utilize the single-link robot arm model from [38].

Example 2. The dynamics of the single-link robot arm model can be expressed in the ensuing second-order nonlinear differential equation:

$$\ddot{\theta}(t) = -\frac{M^{(i)}gL}{I^{(i)}}\sin(\theta(t)) - \frac{D^{(i)}}{I^{(i)}}\dot{\theta}(t) + \frac{1}{I^{(i)}}v(t) + \frac{1}{I^{(i)}}d(t),$$

where, $\theta(t)$ is the angular position of the link, $v(t)$ is the control input, and $d(t)$ represents an external disturbance. The parameter $M^{(i)}$ is the load mass, g is gravitational acceleration, L is the arm length, $I^{(i)}$ is the moment of inertia, and $D^{(i)}$ is the damping coefficient. The discrete parameter set is defined as $\mathbf{p}^{(i)} = (M^{(i)}, I^{(i)}, D^{(i)})$, and it may assume three distinct configurations.

The system parameters for the discrete configurations are given as:

$$\mathbf{p}^1 = (1,1,2), \quad \mathbf{p}^2 = (5,5,2), \quad \mathbf{p}^3 = (10,10,2).$$

Let $\vartheta_1(t) = \theta(t)$ and $\vartheta_2(t) = \dot{\theta}(t)$. The nonlinear term $\sin(\theta(t))$ is approximated as:

$$\sin(\vartheta_1(t)) = \mathfrak{E}_1(\vartheta_1(t))\vartheta_1(t) + \beta\mathfrak{E}_2(\vartheta_1(t))\vartheta_1(t),$$

where the weighting functions are defined as:

$$\mathfrak{E}_1(\vartheta_1(t)) = \begin{cases} \frac{\sin(\vartheta_1(t)) - \beta\vartheta_1(t)}{\vartheta_1(t)(1-\beta)}, & \vartheta_1(t) \neq 0 \\ 1, & \vartheta_1(t) = 0 \end{cases} \text{ and}$$

$$\mathfrak{E}_2(\vartheta_1(t)) = \begin{cases} \frac{\vartheta_1(t) - \sin(\vartheta_1(t))}{\vartheta_1(t)(1-\beta)}, & \vartheta_1(t) \neq 0 \\ 0, & \vartheta_1(t) = 0 \end{cases}.$$

Here, $\beta = \frac{0.01}{\pi}$ and the functions $\mathfrak{E}_1(\vartheta_1(t)), \mathfrak{E}_2(\vartheta_1(t)) \in [0,1]$ satisfy:

$$\mathfrak{E}_1(\vartheta_1(t)) + \mathfrak{E}_2(\vartheta_1(t)) = 1.$$

According to the fuzzy membership representation, the system dynamics can be described by fuzzy rules, such as:

Table 2
Gain values of the sampled robust and fault-tolerant control.

mode	$\mathfrak{H}^1_{j\nu}$	$\mathfrak{H}^2_{j\nu}$
j = 1, ν = 1	$10^3 \times \begin{bmatrix} -6.5248 \\ -2.3108 \end{bmatrix}^T$	$10^6 \times \begin{bmatrix} -7.2522 \\ 1.6887 \end{bmatrix}^T$
j = 1, ν = 2	$10^3 \times \begin{bmatrix} -6.5248 \\ -2.3108 \end{bmatrix}^T$	$10^6 \times \begin{bmatrix} -7.2522 \\ 1.6887 \end{bmatrix}^T$
j = 2, ν = 1	$10^3 \times \begin{bmatrix} -1.9458 \\ -4.3060 \end{bmatrix}^T$	$10^6 \times \begin{bmatrix} -0.5483 \\ -1.9085 \end{bmatrix}^T$
j = 2, ν = 2	$10^3 \times \begin{bmatrix} -1.9458 \\ -4.3060 \end{bmatrix}^T$	$10^6 \times \begin{bmatrix} -0.5483 \\ -1.9085 \end{bmatrix}^T$
j = 3, ν = 1	$10^3 \times \begin{bmatrix} -1.5186 \\ -3.9514 \end{bmatrix}^T$	$10^6 \times \begin{bmatrix} 0.4037 \\ -1.2695 \end{bmatrix}^T$
j = 3, ν = 2	$10^3 \times \begin{bmatrix} -1.5186 \\ -3.9514 \end{bmatrix}^T$	$10^6 \times \begin{bmatrix} 0.4037 \\ -1.2695 \end{bmatrix}^T$

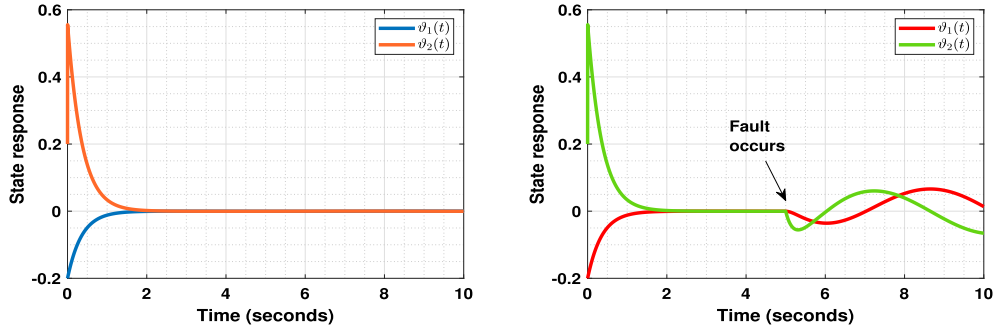

(a) Fault-free environment (b) Fault occurrence

Fig. 8. State response of the system under robust control.

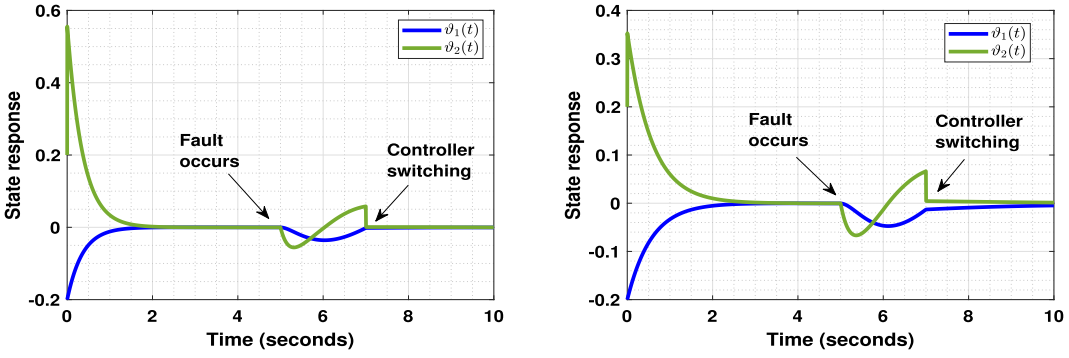

(a) Case (iii) (b) Case (iv)

Fig. 9. State response of the undertaken model through the hybrid control.

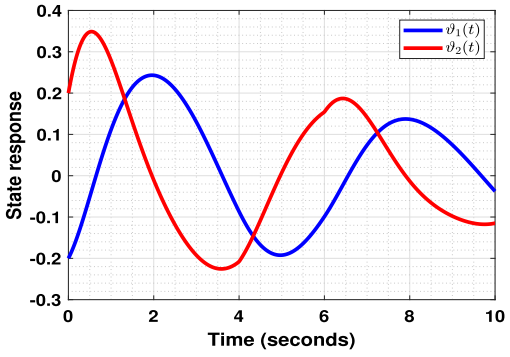

Fig. 10. State response of the model without control.

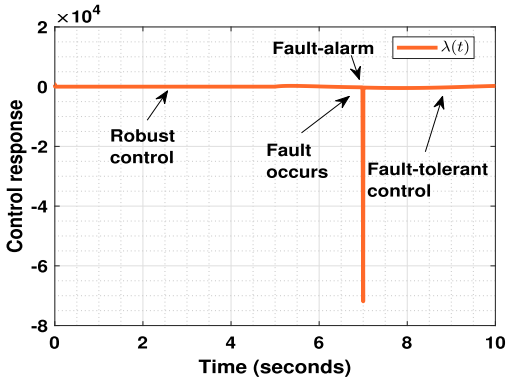

Fig. 11. Hybrid control response.

Rule 1: *IF* $\vartheta_1(t)$ is "approximately 0 rad," *THEN*

$$\dot{\vartheta}(t) = \mathfrak{A}_{j1}\vartheta(t) + \mathfrak{B}_{j1}\lambda(t) + \mathfrak{D}_{j1}\delta(t),$$
$$\xi(t) = \mathfrak{C}_{j1}\vartheta(t),$$

Rule 2: *IF* $\vartheta_1(t)$ is "approximately π or -π rad" *THEN*

$$\dot{\vartheta}(t) = \mathfrak{A}_{j2}\vartheta(t) + \mathfrak{B}_{j2}\lambda(t) + \mathfrak{D}_{j2}\delta(t),$$
$$\xi(t) = \mathfrak{C}_{j2}\vartheta(t),$$

where $\vartheta(t) = [\vartheta_1^T(t)\ \vartheta_2^T(t)]^T$.

Subsequently, the matrix associated with the system are given here:

Subsystem 1:

$$\mathfrak{A}_{11} = \begin{bmatrix} 0 & 1 \\ -gL & -2 \end{bmatrix},\ \mathfrak{B}_{11} = \begin{bmatrix} 0 \\ 1 \end{bmatrix},\ \mathfrak{D}_{11} = \begin{bmatrix} 0 \\ 1 \end{bmatrix},\ \mathfrak{C}_{11} = \begin{bmatrix} 1 \\ 0.1 \end{bmatrix}^T,$$

$$\mathfrak{A}_{12} = \begin{bmatrix} 0 & 1 \\ -\beta gL & -2 \end{bmatrix},\ \mathfrak{B}_{12} = \begin{bmatrix} 0 \\ 1 \end{bmatrix},\ \mathfrak{D}_{12} = \begin{bmatrix} 0 \\ 1 \end{bmatrix},\ \mathfrak{C}_{12} = \begin{bmatrix} 0.9 \\ 0.8 \end{bmatrix}^T,$$

Subsystem 2:

$$\mathfrak{A}_{21} = \begin{bmatrix} 0 & 1 \\ -0.75gL & -1 \end{bmatrix},\ \mathfrak{B}_{21} = \begin{bmatrix} 0 \\ 0.5 \end{bmatrix},\ \mathfrak{D}_{21} = \begin{bmatrix} 0 \\ 0.5 \end{bmatrix},\ \mathfrak{C}_{21} = \begin{bmatrix} 0.5 \\ 0.7 \end{bmatrix}^T,$$

$$\mathfrak{A}_{22} = \begin{bmatrix} 0 & 1 \\ -0.75\beta gL & -1 \end{bmatrix},\ \mathfrak{B}_{22} = \begin{bmatrix} 0 \\ 0.5 \end{bmatrix},\ \mathfrak{D}_{22} = \begin{bmatrix} 0 \\ 0.5 \end{bmatrix},\ \mathfrak{C}_{22} = \begin{bmatrix} 0.6 \\ 0.5 \end{bmatrix}^T,$$

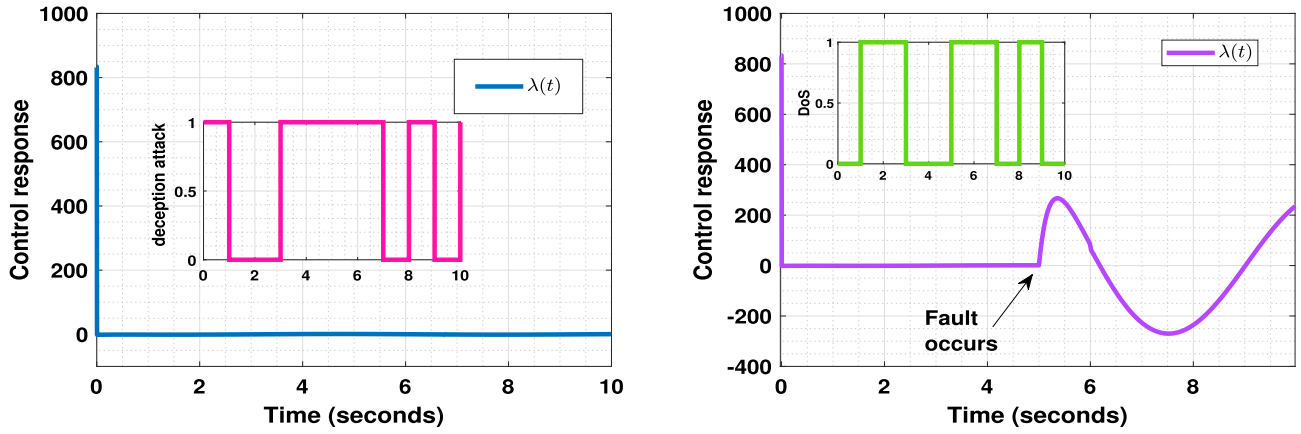

(a) Fault-free case (b) Fault case

Fig. 12. Control trajectories under robust control.

Subsystem 3:

$$\mathfrak{A}_{31} = \begin{bmatrix} 0 & 1 \\ -0.8gL & -0.8 \end{bmatrix}, \ \mathfrak{B}_{31} = \begin{bmatrix} 0 \\ 0.4 \end{bmatrix}, \ \mathfrak{D}_{31} = \begin{bmatrix} 0 \\ 0.4 \end{bmatrix}, \ \mathfrak{C}_{31} = \begin{bmatrix} 0.4 \\ 0.6 \end{bmatrix}^T,$$

$$\mathfrak{A}_{32} = \begin{bmatrix} 0 & 1 \\ -0.8\beta gL & -0.8 \end{bmatrix}, \ \mathfrak{B}_{32} = \begin{bmatrix} 0 \\ 0.4 \end{bmatrix}, \ \mathfrak{D}_{32} = \begin{bmatrix} 0 \\ 0.4 \end{bmatrix}, \ \mathfrak{C}_{32} = \begin{bmatrix} 0.5 \\ 0.4 \end{bmatrix}^T,$$

where $g = 9.81$ and $L = 0.5$. Moreover, the interval for the fault is chosen as $\mathfrak{G} \in [0.1, 0.2]$. The scalars in the finite-time notion are picked as $C_1 = 0.2, C_2 = 5, \mathcal{G}_{\text{to}} = 10$ and $\delta_b = 0.9$. The parameters of the sampled-data control are $\mathfrak{y}_1 = 0.0001$ and $\mathfrak{y}_2 = 0.15$. The leftover parameters that constitute the feasibility duty are designated as $\bar{\alpha} = 0.5$, $\bar{\beta} = 0.5$, $\mathcal{F} = diag\{0.52, 0.52\}$, $\mathcal{F}_1 = -0.82$, $\mathcal{F}_2 = 0.87$, $\mathcal{F}_3 = 0.68$ and $\gamma = 1.6$. After carrying out all of these variables in the framework of MATLAB and addressing the criteria (81)–(85) derived in the corollary 1, we obtain the gain matrices of the developed hybrid controller which is shown in the Table 2.

Following the closing out of the feasibility work, the subsequent beginning of the simulation activity requires the following functions and criteria. The disturbance and attack functions are selected as $\delta(t) = 0.9\sin(t)$ and $\mathfrak{f}(\vartheta(t)) = 0.52\sin(\vartheta(t))$. Further, the initial state is given as $\vartheta(0) = \begin{bmatrix} -0.2 & 0.2 \end{bmatrix}^T$.

Subsequently, by employing the matrices, scalars, and conditions outlined earlier, the simulation task is carried out under the sampling time 0.01, and the outcomes of the illustrations are presented in Figs. 8–14. Specifically, the state curves of the undertaken model in the context of the sampled robust control rule are depicted in Fig. 8. In particular, the state trajectories of the examined model under the sampled robust control law in the absence of faults are illustrated in Fig. 8(a). Conversely, in Fig. 8(b) is apparently visible that, when the system encounters failures within the context of sampled robust control, the system states diverge, which indicates that the implemented control law is not good enough in addressing the impacts of faults. Furthermore, the state outcomes of the conducted model through the sampled hybrid control under two cases are illustrated in Fig. 9. Precisely, Fig. 9 makes it straightforward that, shortly after a fault occurs in the control law, the controller shifts to a fault-tolerant mode, working with a fault alarm indication mechanism. This visual representation shows how the state performance functions smoothly when the system is under the fault-tolerant mode, highlighting the significance of the developed hybrid control law. Added to this, from Fig. 9(a), we can see that, when the designed control is implemented, the trajectories of the investigated model have faster convergence rate and transits the control law rapidly whereas in Fig. 9(b), under the traditional hybrid control method, the recovery is slower and less smooth,

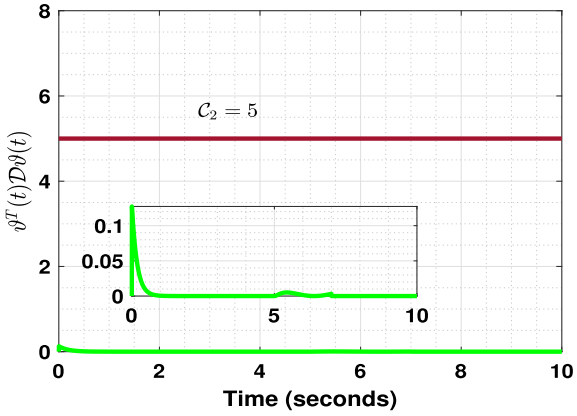

Fig. 13. Time profile of state trajectory.

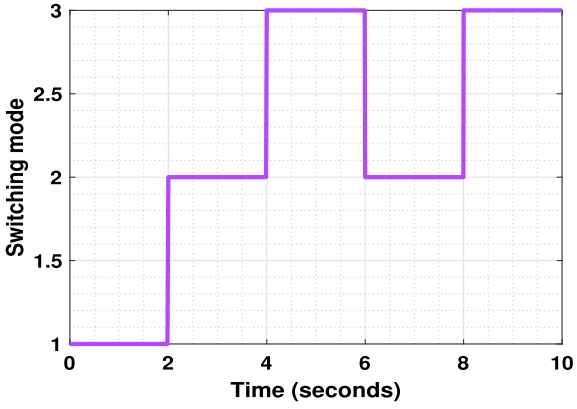

Fig. 14. Time profile of switching law.

which pinpoints the necessity of establishing a secured hybrid control technique and shows how the considered hybrid cyber attacks have made a considerable impact on the performance of the system states. Further, by leaving out the control law from the model's comprehensive framework, the trajectories of the states are illustrated in Fig. 10, where the divergence of the states highlights the crucial nature of formulating the control law for the proposed model. Added to that, hybrid control law trajectories are offered in Fig. 11. Furthermore, the control

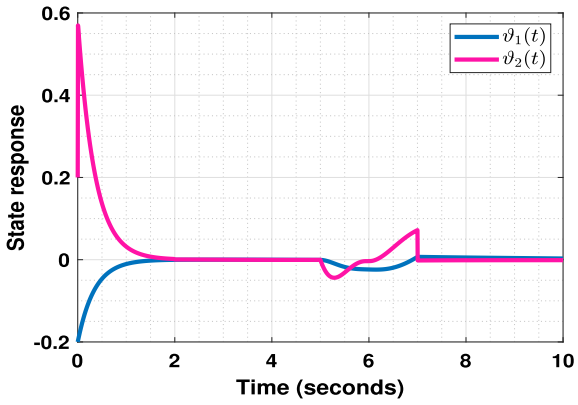

Fig. 15. Time profile of state trajectory under case (v).

outcomes when the system is fault-free and when it is impacted by faults are portrayed in Fig. 12. Also, the random characteristics of the deception and DoS attacks are offered in Fig. 12(a) and (b), respectively. And, the curves of $\vartheta^T(t)D\vartheta(t)$ are depicted in Fig. 13, wherein states are under the specified bound that ensures the finite-time boundedness of the examined system. Also, the switching mode $\zeta(t)$ for the examined model is portrayed in Fig. 14. In the closing portion, Case (v): State responses of the single-link robot arm under a wind-like disturbance $\delta(t) = 0.9\sin(t)$ with a half sine-gust on $t \in [5.0, 6.01]$ are presented in Fig. 15. The proposed secured hybrid controller attenuates the induced oscillations and maintains the states.

In brief, the data generated through simulation reveals that when the system encounters actuator failure, the depicted controller begins operating decisively in response to the signal from the fault alarm system. Additionally, the assessment reveals that the fault alarm-based hybrid controller is capable of effectively handling unforeseen actuator failures within the system. It also supports the system in maintaining stability in the face of cyberattacks, external disturbances and actuator failures.

5. Conclusion

This paper looked into the sampled hybrid control scheme problems for NSFSs over a finite horizon, considering numerous prone facets. In detail, actuator failures, hybrid cyber attacks, external disturbances and time-varying delays are taken into account. Further, a hybrid control law has been developed by blending robust and fault-tolerant mechanisms, whereby shifting between controllers is governed by a fault alarm strategy. The most significant feature of this controller is that robust control will be executed when the system is free of fault and transitioned to fault-tolerant mode upon encountering actuator failures. Furthermore, by factoring the sampling information from $\vartheta(t_\ell)$ to $\vartheta(t)$ and $\vartheta(t)$ to $\vartheta(t_{\ell+1})$, a two-sided looped Lyapunov functional is formulated. After that, adequate constraints are formed with the support of LMIs and the framed looped functional, which are certain that the primary purpose of this inquiry is attained. Moreover, an extended dissipative framework is put to use for lowering the negative consequences of external disturbances. The investigation wraps up with numerical examples, one of which is a single-link robot arm model, along with findings from simulation that point out the prospective benefits and relevance of the devised control laws and theoretical discoveries. Despite its strengths, this study has limitations. First, the residual-based fault detector relies on a fixed bound; its sensitivity and false-alarm rate depend on the accuracy of this bound, and may worsen if the actual disturbance occasionally exceeds it. Second, the controller is synthesized for single actuator faults; extensions to sensor faults and simultaneous multi-faults are not covered here. In our future endeavours, beyond the present residual-based detection framework, we will investigate a data-driven, parameterized threshold design for fault detection under event-trigger sampling and multiple disturbance channels.

CRediT authorship contribution statement

N. Aravinth: Writing – original draft. **R. Sakthivel:** Writing – review & editing, Validation. **O.M. Kwon:** Writing – review & editing, Validation.

Declaration of competing interest

The authors declare that they have no known competing financial interests or personal relationships that could have appeared to influence the work reported in this paper.

Acknowledgements

This work was supported by the Basic Science Research Program through the National Research Foundation of Korea (NRF) funded by the Ministry of Education (RS-2020-NR049604) and partially supported by Innovative Human Resource Development for Local Intellectualization program through the Institute of Information & Communications Technology Planning & Evaluation (IITP) grant funded by the Korea government (MSIT) (IITP-2025-RS-2020-II201462, 50 %).

Data availability statement

Data sharing is not applicable to this article as no datasets were generated or analyzed during the current study.

References

[1] Zhang L, Zhao Z, Ma Z, Zhao N. Prescribed performance adaptive neural event-triggered control for switched nonlinear cyber-physical systems under deception attacks. Neural Netw 2024;179:106586.
[2] Wang W, Lian J, Jia P, Chen K. Finite-time prescribed performance adaptive control for a class of switched uncertain nonlinear systems. IEEE Trans Autom Sci Eng 2025;22:13224–35.
[3] Zong G, Yang D, Lam J, Song X. Fault-tolerant control of switched LPV systems: a bumpless transfer approach. IEEE ASME Trans Mechatronics 2021;27:1436–46.
[4] Wang H, Xu K, Zhang H. Adaptive finite-time tracking control of nonlinear systems with dynamics uncertainties. IEEE Trans Autom Control 2022;68:5737–44.
[5] He X, Li X, Song S. Prescribed-time stabilization of nonlinear systems via impulsive regulation. IEEE Trans Syst Man Cybern Syst 2022;53:981–5.
[6] Ge C, Liu Z, Wang L, Liu Y. Improved stability criteria of TS fuzzy systems with sampled-data-based dissipative control. Appl Math Comput 2022;424:127047.
[7] Ku CC, Chang WJ, Tsai MH, Lee YC. Observer-based proportional derivative fuzzy control for singular takagi-sugeno fuzzy systems. Inf Sci 2021;570:815–30.
[8] Wu Y, Hu S, Li W. Exponential stability of stochastic takagi-sugeno fuzzy systems under intermittent dynamic event-triggered control. IEEE Trans Fuzzy Syst 2021;30:1648–59.
[9] Zhao N, Zhao X, Zong G, Xu N. Resilient event-triggered filtering for networked switched TS fuzzy systems under denial-of-service attacks. IEEE Trans Fuzzy Syst 2023;32:2140–52.
[10] Sun X, Yang D, Zong G. Annular finite-time H_∞ control of switched fuzzy systems: a switching dynamic event-triggered control approach, nonlinear analysis. Hybrid Systems 2021;41:101050.
[11] Cui D, Chadli M, Xiang Z. Fuzzy fault-tolerant predefined-time control for switched systems: a singularity-free method. IEEE Trans Fuzzy Syst 2023;32:1223–32.
[12] Tang L, Yang M, Liu YJ, Tong S. Adaptive output feedback fuzzy fault-tolerant control for nonlinear full-state-constrained switched systems. IEEE Trans Cybern 2021;53:2325–34.
[13] Li JN, Xu YF, Bao WD, Xu XB. Passivity and fault alarm-based hybrid control for a markovian jump delayed system with actuator failures. IEEE Access 2017;6:797805.
[14] Li JN, Xu YF, Gu KY, Li LS, Xu XB. Mixed passive/H_∞ hybrid control for delayed markovian jump system with actuator constraints and fault alarm. Int J Robust Nonlinear Control 2018;28:6016–37.
[15] Li Y, Yu K. Adaptive fuzzy decentralized sampled-data control for large-scale nonlinear systems. IEEE Trans Fuzzy Syst 2021;30:1809–22.
[16] Yan S, Gu Z, Park JH, Xie X. Sampled memory-event-triggered fuzzy load frequency control for wind power systems subject to outliers and transmission delays. IEEE Trans Cybern 2022;53:4043–53.
[17] Park JH, Park PG. An extended looped-functional for stability analysis of sampled-data systems. Int J Robust Nonlinear Control 2020;30:7962–9.
[18] Suh YS. Stability and stabilization of nonuniform sampling systems. Automatica 2008;44:3222–6.
[19] Naghshtabrizi P, Hespanha JP, Teel AR. Exponential stability of impulsive systems with application to uncertain sampled-data systems. Syst Control Lett 2008;57:378–85.

[20] Lian J, Li C, Xia B. Sampled-data control of switched linear systems with application to an F-18 aircraft. IEEE Trans Ind Electron 2017;64:1332–40.
[21] Zeng HB, Teo KL, He Y. A new looped-functional for stability analysis of sampled-data systems. Automatica 2017;82:328–31.
[22] Davo MA, Banos A, Gouaisbaut F, Tarbouriech S, Seuret A. Stability analysis of linear impulsive delay dynamical systems via looped-functionals. Automatica 2017;81:107–14.
[23] Hua C, Wu S, Guan X. Stabilization of TS fuzzy system with time delay under sampled-data control using a new looped-functional. IEEE Trans Fuzzy Syst 2019;28:400–7.
[24] Huan M, Li C. Stability analysis of state-dependent impulsive systems via a new two-sided looped functional, chaos. Solitons Fractals 2022;155:111758.
[25] Li JZ, Zhang YY, Zeng HB. Stability and L_2-gain analysis for impulsive delay systems via two-sided looped-functional. Int J Control Autom Syst 2023;21:92–934.
[26] Li X, She K, Shi K, Cheng J, Qiu K, Peng Z. HMM-based asynchronous synthesis for interval type-2 fuzzy semi-markovian jump systems with its applications: a bilateral looped functional methodology. Expert Syst Appl 2024;240:122213.
[27] Cai X, Shi K, Sun Y, Cao J, Wen S, Chen P, Tian Z. Dual-channel ncss performance error estimation under DOS attacks and intelligent control supervised by machine learning to AGV application. IEEE Trans on Transp Electrification 2023;10:4882–93.
[28] He H, Qi W, Yan H, Cheng J, Shi K. Adaptive fuzzy resilient control for switched systems with state constraints under deception attacks. Information Sciences 2023;621:596–610.
[29] Jiao S, Xu S, Park JH. Hybrid-triggered-based control against denial-of-service attacks for fuzzy switched systems with persistent dwell-time. IEEE Trans Fuzzy Syst 2024;32:710–20.
[30] Liu J, Wang Y, Cao J, Yue D, Xie X. Secure adaptive-event-triggered filter design with input constraint and hybrid cyber attack. IEEE Trans Cybern 2020;51:4000–10.
[31] Wang Y, Zhang S, Zhuang G, Shao M. Secure dynamic-event-based filtering for descriptor nonhomogeneous markovian jump cyber-physical systems against hybrid cyber-attacks. Int J Adapt Control Signal Process 2024;38:3422–55.
[32] Chen H, Zong G, Gao F, Shi Y. Probabilistic event-triggered policy for extended dissipative finite-time control of mjss under cyber-attacks and actuator failures. IEEE Trans Autom Control 2023;68:7803–10.
[33] Wei F, Xu N, Huang S, Cao Y. Disturbance observer-based adaptive neural finite-time control for nonstrict-feedback nonlinear systems with input delay. Trans Inst Meas Control 2025;47:1172–87.
[34] Meng B, Liu W, Qi X. Disturbance and state observer-based adaptive finite-time control for quantized nonlinear systems with unknown control directions. J Frankl Inst 2022;359:2906–31.
[35] Gao H, Xia J, Zhuang G, Wang Z, Sun Q. Nonfragile finite-time extended dissipative control for a class of uncertain switched neutral systems. Complexity 2017;1:6581308.
[36] Samidurai R, Sriraman R, Cao J, Tu Z. Nonfragile stabilization for uncertain system with interval time-varying delays via a new double integral inequality. Math Methods Appl Sci 2018;41:6272–87.
[37] Zamart C, Botmart T, Weera W, Charoensin S. New delay-dependent conditions for finite-time extended dissipativity based non-fragile feedback control for neural networks with mixed interval time-varying delays. Math Comput Simul 2022;201:684–713.
[38] Zheng Q, Xu S, Du B. Asynchronous resilent state estimation of switched fuzzy systems with multiple state impulsive jumps. IEEE Trans Cybern 2023;53:7966–79.